NASA TN D-798

NASA TN D-798

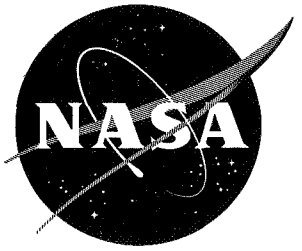

TECHNICAL NOTE

D-798

SOME SIMPLE SOLUTIONS TO THE PROBLEM OF PREDICTING BOUNDARY-LAYER SELF-INDUCED PRESSURES

By Mitchel H. Bertram and Thomas A. Blackstock

Langley Research Center
Langley Field, Va.

NATIONAL AERONAUTICS AND SPACE ADMINISTRATION

WASHINGTON April 1961

CONTENTS

NATIONAL AERONAUTICS AND SPACE ADMINISTRATION

TECHNICAL NOTE D-798

SOME SIMPLE SOLUTIONS TO THE PROBLEM OF PREDICTING BOUNDARY-LAYER SELF-INDUCED PRESSURES

By Mitchel H. Bertram and Thomas A. Blackstock

SUMMARY

Simplified theoretical approaches are shown, based on hypersonic similarity boundary-layer theory, which allow reasonably accurate estimates to be made of the surface pressures on plates on which viscous effects are important. The consideration of viscous effects includes the cases where curved surfaces, stream pressure gradients, and leading-edge bluntness are important factors.

INTRODUCTION

As the Mach number increases into the hypersonic range large pressure and temperature gradients can be induced on a flat plate by leading-edge bluntness and boundary-layer displacement effects. Any curvature to the plate surface simply adds still another complicating factor to the flow picture, and there may be any combination of these factors. In addition to the effect of these induced pressures on loading, the increased pressures can have an important effect on the skin friction and heat transfer on the plate surface.

The purpose of this paper is to show the simplified theoretical approaches which are presently available and which allow reasonably accurate estimates to be made of the surface pressures on plates on which viscous effects are important and where surface curvature, stream pressure gradients, and leading-edge bluntness can be contributory factors.

SYMBOLS

a constant

$C = \mu_w T_\infty / \mu_\infty T_w$

d	diameter of cylinder
G	$f(T_w, T_r, \gamma, M_\infty)$ in equation for laminar boundary-layer growth (see eqs. (3) and (14))
j	index number (0 for planar model, 1 for cylindrical model)
K	hypersonic similarity deflection angle (M_∞ · deflection angle)
K_δ	hypersonic similarity deflection angle using slope at edge of boundary layer
K_4	coefficient in hypersonic-similarity-theory-laminar-boundary-layer growth equation (see eq. (2) and fig. 1)
k	nose drag coefficient
M	Mach number
m	exponent in power equation for surface coordinates of curved plate $(y \propto x^m)$
N_{Kn}	Knudsen number
N_{Pr}	Prandtl number
n	exponent in power equation for surface pressure variation with x
P	ratio of local surface pressure to free-stream static pressure
p	pressure
R	Reynolds number
R_t, R_d	Reynolds number based on undisturbed free-stream conditions and leading-edge thickness or rod diameter, respectively
T	absolute temperature
t	leading-edge thickness
x	distance along axis of flat plate from leading edge
w	model span

α angle of inclination of flat plate relative to free-stream, flow direction

γ ratio of specific heats

δ boundary-layer thickness (see eq. (2))

ϵ correction factor for γ in bluntness-induced-pressure equation (see eq. (41))

μ dynamic viscosity

ξ coefficient in induced-pressure equation for rod (see eq. (50))

$\bar{\chi}$ viscous interaction parameter $\bar{\chi} \equiv \frac{M_\infty^3 \sqrt{C}}{\sqrt{R_{\infty,x}}}$

ω local surface slope

Subscripts:

b nose bluntness induced

i inviscid

r adiabatic wall

v viscous induced

w wall

x surface distance

∞ free stream

0 stagnation

2 local inviscid pressure

A prime designates the first derivative with respect to the subscript.

Superscripts in parentheses refer to the order of an equation developed in series.

SOME SPECIAL SOLUTIONS FOR THE SELF-INDUCED PRESSURE GRADIENT

Useful results may be obtained if the similarity theory for a boundary layer in hypersonic flow (ref. 1) is used as a basis for predicting self-induced pressures to a higher order than may be obtained from the so-called "weak-interaction" or "strong-interaction" solutions. (See ref. 2 for a discussion of these theories.) First, consider the boundary-layer thickness itself in hypersonic flow. To satisfy the requirements of this hypersonic similarity theory, a pressure variation at the edge of the boundary layer is postulated as follows:

$$p_w \propto x^n \tag{1}$$

Then according to the hypersonic similarity theory (ref. 1) the boundary-layer thickness is (assuming Prandtl number unity in the derivation)

$$\delta = GK_4(\gamma,n)\frac{M_\infty^2\sqrt{C}}{\sqrt{P}}\frac{x}{\sqrt{R_{\infty,x}}} \tag{2}$$

where

$$G = 1.7208\frac{\gamma - 1}{2}\left(\frac{T_w}{T_0} + 0.3859\right) \tag{3}$$

and $K_4(\gamma,n)$ is the coefficient determined from hypersonic similarity theory. The variation of K_4 with negative exponents in the pressure-variation law (favorable pressure gradients) is shown in figure 1. The curves shown are different from those in reference 1 because additional values from reference 3 of the integral function used to obtain K_4 have been utilized to obtain more accurate fairings of the integral function.

If hypersonic tangent-wedge theory (ref. 4) with the slope of the outer edge of the boundary layer as the effective wedge angle is assumed to be sufficient to determine local surface pressures then

$$P = f\left(M_\infty \delta_x'\right) = f\left(K_\delta\right) \tag{4}$$

The boundary-layer slope is upon differentiation of equation (2) (with K_4 assumed to be constant)

$$\delta_x' = \frac{GK_4 M_\infty^2 \sqrt{C}}{2\sqrt{PR_{\infty,x}}}\left(1 - \frac{x}{P}\frac{dP}{dx}\right) \tag{5}$$

or in terms of the Lees-Probstein interaction parameter $\bar{\chi}$ (ref. 5) where

$$\bar{\chi}_\infty \equiv \frac{M_\infty^3 \sqrt{C}}{\sqrt{R_{\infty,x}}} \tag{6}$$

the hypersonic similarity deflection angle may be written

$$K_\delta = \frac{K_4}{2}\frac{G\bar{\chi}_\infty}{\sqrt{P}}\left(1 + \frac{\bar{\chi}_\infty}{2P}\frac{dP}{d\bar{\chi}_\infty}\right) \tag{7}$$

Now consider which values of the pressure-law exponent n are of interest if self-induced pressures only are to be considered. The variation of the local value of the exponent n with self-induced pressure ratio P is shown in figure 2. The value of n is zero at P = 1 and at increasingly large pressures the curve of n is asymptotic to -0.5, the value obtained from strong-interaction theory. The values of n shown in figure 2 were obtained by assuming that the pressure is linear in $\bar{\chi}$ with the following form (developed in more detail in a later section)

$$P = 1 + a\bar{\chi} \tag{8}$$

since for any function (of x, say) the local value of the exponent in a power-law fit to the function may be expressed as $n = \frac{xf'(x)}{f(x)}$, then for equation (8) f(x) is $(1 + a\bar{\chi})$ and thus the exponent n as a function of pressure ratio is given by

$$n = -\frac{1}{2}\frac{P - 1}{P} \tag{9}$$

Figure 1 shows that in helium ($\gamma = 5/3$) the coefficient K_4 is essentially unity (error generally less than 2 percent) in the range $0 > n > -0.5$ and in air ($\gamma = 7/5$) the maximum deviation from unity is about 10 percent.

Weak Interactions

First consider equation (7) in the light of weak-interaction theory. From hypersonic small-perturbation theory (see ref. 4)

$$p^{(2)} = 1 + \gamma K_\delta + \frac{\gamma(\gamma + 1)}{4} K_\delta^2 \tag{10}$$

Assume that a first-order correction for the local pressure is sufficient in equation (7). That is, the value of P to be inserted in equation (10) will be obtained from the first-order solution to the weak-interaction boundary-layer problem (ref. 5) where

$$p^{(1)} = 1 + \frac{\gamma G \bar{X}_\infty}{2} \tag{11}$$

Substituting equation (11) into equation (7) with $\left(K_4 = 1\right)$ and then this combination into equation (10) results in the following relation

$$p^{(2)} = 1 + \frac{\frac{\gamma G \bar{X}_\infty}{2}}{\sqrt{1 + \frac{\gamma G \bar{X}_\infty}{2}}}\left[1 + \frac{\frac{\gamma G \bar{X}_\infty}{2}}{2\left(1 + \frac{\gamma G \bar{X}_\infty}{2}\right)}\right] + \frac{\gamma + 1}{4\gamma} \frac{\left(\frac{\gamma G \bar{X}_\infty}{2}\right)^2}{\left(1 + \frac{\gamma G \bar{X}_\infty}{2}\right)}\left[1 + \frac{\frac{\gamma G \bar{X}_\infty}{2}}{2\left(1 + \frac{\gamma G \bar{X}_\infty}{2}\right)}\right]^2 \tag{12}$$

Equation (12) may be compared with the original Lees-Probstein equation (ref. 5) for second-order weak interaction which in the present nomenclature may be written as follows:

$$P^{(2)} = 1 + \frac{\gamma G}{2}\bar{X}_\infty + \frac{\gamma + 1}{4\gamma}\left(\frac{\gamma G}{2}\bar{X}_\infty\right)^2 \tag{13}$$

Equation (13) may be derived readily from equation (10) by utilizing equation (7) and $n = 0$.

Figure 3 has been prepared to show the difference between the use of equations (12) and (13) in the case mentioned previously where the boundary-layer thickness coefficient K_4 is essentially unity, that is, the flat plate in helium. In addition to the Prandtl number one solution, curves for Prandtl number 0.725 are also shown for which the preceding development is taken to hold except that G is given by the following equation adapted from reference 6:

$$G = 1.648\frac{\gamma - 1}{2}\left(\frac{T_w}{T_r} + 0.352\right) \tag{14}$$

The reduction in induced effects due to the first-order correction for local pressure is certainly significant and appears to be corroborated by experimental results obtained by Henderson and Johnston on a 5° wedge tested in helium (ref. 7). In figure 3 both $\bar{X}$ and the pressure-difference ratio are based on the inviscid conditions that would occur on a wedge having a sharp leading edge were there no boundary layer present. For the two stations nearest the leading edge the experimental data are shown both as measured and with an increment in pressure subtracted to account for leading-edge bluntness. This increment ascribed to leading-edge-bluntness effects is estimated from a correlation of characteristics solutions for the flat plate with a sonic-wedge leading edge at angle of attack (ref. 8) by parameters suggested by Chernyi (ref. 9) and based on the assumption that the boundary-layer-induced and bluntness-induced effects may be treated independently. The effect of leading-edge bluntness is indicated to be small. The 10° wedge data also shown on this plot were obtained at too low a value of $\bar{X}$ to aid in distinguishing between theories considering data uncertainties.

Strong Interactions

Thus far the discussion has been restricted to considering relatively small induced pressures, that is, restricted more or less to the weak-interaction regime of self-induced pressures. Assuming that the tangent-wedge approach is still applicable, a more general approach, insofar as the basic pressure equation used is concerned, will now be attempted. In this case the hypersonic equation given by Lees (ref. 4)

will be used. This equation is in terms of boundary-layer slope

$$P = 1 + \frac{\gamma(\gamma + 1)}{4}K_\delta^2 + \gamma K_\delta \sqrt{1 + \left(\frac{\gamma + 1}{4}K_\delta\right)^2} \tag{15}$$

Based on equation (7), with $K_4 = 1$ and with equation (15), calculations have been carried out for helium. These calculations were made by iteration for a given value of $\bar{X}$ by assuming for each iteration that the pressure ratio is a linear function of $\bar{X}$ starting with the result from strong-interaction theory. (See refs. 4 and 1.) In this way the results are easily calculated. Iterations are obtained by averaging the assumed pressure ratio and the pressure ratio resulting from this assumption. This average is used to start the next iteration. The results are shown in figure 4. The convergence is rapid. The use of the more accurate pressure law (eq. (15)) makes only a small difference from the results obtained by using the expansion of equation (15) for large K_δ or

$$P^{(0)} = \frac{\gamma(\gamma + 1)}{2}K_\delta^2 \tag{16}$$

The differential equation which results when equation (16) is substituted into equation (7) may be solved to give the asymptotic solution known as strong-interaction theory

$$P^{(0)} = \frac{3}{4}\sqrt{\frac{\gamma(\gamma + 1)}{2}}\,G\bar{X}\left(K_4\right)_{n=-1/2} \tag{17}$$

where G is given by equation (3) and the required values of K_4 are given in figure 1. A comparison of the complete hypersonic equation (eq. (15)) with its "strong" shock approximation (eq. (16)) and its "weak" shock approximation (eq. (10)), is shown in figure 5.

The result of the iteration procedure utilizing equation (15) and equation (7) will hereafter be referred to as the "complete theory" (for the sake of briefness even though fundamental completeness is not implied). The results from the complete theory are the same as those from equation (12) for values of $G\bar{X}$ less than approximately 3. For $G\bar{X}$ greater than approximately 1 the curve for the variation of P with $G\bar{X}$ is essentially linear and may be accurately represented by the equation

$$P = 0.83 + \frac{3}{4}\sqrt{\frac{\gamma(\gamma + 1)}{2}}\,G\bar{X} \tag{18}$$

Interestingly enough, for practical purposes this result could have been obtained from equation (17) if K_4 were assumed to be unity and $P^{(0)} = P - 1$, even though equation (16) deviates markedly from equation (15) at the lower pressure ratios. For $P > 4$ the induced-presssure ratio can in general be taken as

$$P \approx 1 + \frac{3}{4}\sqrt{\frac{\gamma(\gamma + 1)}{2}}\,G\bar{X}\left(K_4\right)_{n=-1/2} \tag{19}$$

while for $P < 4$ equation (12) should be adequate and, in general, data should lie in the region defined by equations (12) and (19). A comparison between equations (12), (13), (19), and the complete theory (essentially eq. (18) is shown in figure 4.

Consider now the insulated plate in air where the value of the coefficient K_4 deviates by an appreciable amount from the value unity. (See fig. 1.) Here the fact that K_4 is greater than 1 offsets, to some extent, the result of $P > 1$ on the boundary-layer thickness. (See eq. (2).) Thus in the low $\bar{X}$ range the actual induced pressures will be expected to be between the values given by equations (12) and (13), but closer to the values from equation (12). As $\bar{X}$ increases the actual pressure would be expected to approach the complete theory with a constant value of $K_4 = 1.1$ which is essentially equation (19).

These various theories are shown in figure 6 with applicable data. Shown are Kendall's data from an insulated flat plate at $M_\infty = 5.8$ (ref. 10) and data obtained in the Langley 11-inch hypersonic tunnel at $M_\infty = 9.6$ on a noninsulated plate with a temperature gradient for which the data have been corrected to the insulated plate case as described in reference 2. At $M_\infty = 9.6$ data both with the plate surface alined with the flow and at an angle of attack have been obtained. (A portion of this data has previously been reported in refs. 11, 12, and 13.) The data for zero angle of attack extend the data given in reference 2 and are believed to be more accurate while angle of attack has been used to extend the range of $\bar{X}$ and to give an additional check on the validity of the correction to insulated plate conditions. At angle of attack the local inviscid Mach number departs appreciably from 9.6 as shown in figure 6(b). The original data were picked at a time when the temperature distribution on the plate was the same for all Reynolds numbers and

angles of attack. This temperature distribution is shown in references 11 and 12.

At zero angle of attack (fig. 6(a)) there is good agreement between Kendall's data and present data in the range where they overlap. The data points in general are slightly above the curve for weak-interaction theory with the local pressure correction (eq. (12)) but approach the curve for "complete theory" with $K_4 = 1.1$ at the higher values of $\bar{\chi}$. The pressure data at angles of attack (fig. 6(b)) show good agreement with the data at zero angle of attack, at least for values of $\bar{\chi}$ up to about 10, and indicate that the complete theory with $K_4 = 1.1$ (or eq. (19)) is adequate at least in the range of $\bar{\chi}$ shown.

BOUNDARY-LAYER-INDUCED EFFECTS IN A NON-SELF-INDUCED PRESSURE GRADIENT

Strong Non-Self-Induced Pressure Gradient

Effect of wall curvature.- First, with equation (1) as a requirement, the slope of the edge of the boundary layer (eq. (4)) in hypersonic similarity form may be written as

$$K_\delta \equiv M_\infty \delta_x' = \frac{G}{2} \frac{\bar{\chi}_\infty}{\sqrt{p_2/p_\infty}}(1 - n)K_4 \tag{20}$$

Then assume that the boundary layer is growing on a surface of sufficient curvature so that equation (16) well represents the pressures induced by the surface slope alone. In general, a change in the slope of the surface induces a pressure rise above the pressure that would have existed as follows (from a finite perturbation on eq. (16)):

$$\frac{p_w - p_2}{p_\infty} = \frac{\gamma(\gamma + 1)}{2}\left[2(\Delta K)K + (\Delta K)^2\right] \tag{21}$$

where $K = M_\infty \omega$. If $\Delta K \equiv K_\delta$ and K_δ is assumed to be small then equation (21) with equations (20) and (16) gives

$$\frac{p_w - p_2}{p_\infty} = \sqrt{\frac{2(\gamma + 1)}{\gamma}}\, G\bar{X}_\infty (1 - n)K_4 \tag{22}$$

which, since $2(\Delta K)K \gg (\Delta K)^2$, holds for

$$\frac{p_2}{p_\infty} \gg \sqrt{\frac{\gamma + 1}{8\gamma}}\, \frac{\gamma G}{2}\bar{X}_\infty (1 - n)K_4$$

where n is obtained from $\frac{p_2}{p_\infty} = f(\omega)$ in the form of equation (16). Equation (22) does not reduce to equation (17) when $n = -1/2$, since the self-induced effect is derived as a small perturbation on a pre-existing pressure gradient.

If the ratio of the local wall pressure, with the self-induced effect included, to the inviscid local pressure is desired equation (22) may be written as

$$\frac{p_w}{p_2} = 1 + \sqrt{\frac{2(\gamma + 1)}{\gamma}}\, \frac{\gamma G}{2}\, \frac{\bar{X}_\infty}{p_2/p_\infty} (1 - n)K_4 \tag{23}$$

which has the same limitation as equation (22). Now for hypersonic flow

$$\frac{\bar{X}_2}{\bar{X}_\infty} = \sqrt{\frac{T_\infty}{T_2}\, \frac{p_\infty}{p_2}} \tag{24}$$

For an oblique shock compression with pressure ratios not too close to unity

$$\frac{T_2}{T_\infty} = \frac{\gamma - 1}{\gamma + 1}\, \frac{p_2}{p_\infty} + 1 \tag{25}$$

If, further, the unity term in equation (25) can be neglected then

$$\frac{\bar{X}_2}{\bar{X}_\infty} \approx \frac{p_\infty}{p_2} \sqrt{\frac{\gamma + 1}{\gamma - 1}} \tag{26}$$

Then in terms of inviscid local conditions equation (23) with equation (26) becomes

$$\frac{p_w}{p_2} = 1 + \sqrt{\frac{2(\gamma - 1)}{\gamma}} \frac{\gamma G \bar{X}_2}{2}(1 - n)K_4 \tag{27}$$

Equation (23) may also be presented in terms of surface slope by using equation (16) or

$$\frac{p_w}{p_2} = 1 + \sqrt{\frac{2}{\gamma(\gamma + 1)}} \frac{G\bar{X}_\infty}{K^2}(1 - n)K_4 \qquad \left(K^2 \gg \frac{G}{4}\bar{X}_\infty \sqrt{\frac{2}{\gamma(\gamma + 1)}}(1 - n)K_4\right) \tag{28}$$

The externally imposed pressure gradient.- The case where the pressure gradient is externally imposed may also be simply treated. Again it is assumed that the increase in surface pressure is small compared to the inviscid local pressure. The local pressure ratio is assumed to be given by the first-order form of equation (10), which is

$$\frac{p_w}{p_2} = 1 + \gamma K_{\delta,2} \tag{29}$$

where the required form of equation (7) is

$$K_{\delta,2} \equiv M_2 \delta_x' = \frac{G}{2} \frac{\bar{X}_\infty}{\sqrt{p_2/p_\infty}} \frac{M_2}{M_\infty}(1 - n)K_4 \tag{30}$$

and with isentropic external flow or isentropic compression on a curved plate

$$K_{\delta,2} = \frac{G}{2} \frac{\bar{X}_\infty}{\left(\frac{p_2}{p_\infty}\right)^{\frac{2\gamma-1}{2\gamma}}}(1 - n)K_4 \tag{31}$$

in which the variation of the local inviscid pressure ratio p_2/p_∞, with surface distance has the form of equation (1) and the value of $(1 - n)K_4$ is obtained from this pressure law. In this case ∞ refers to some convenient reference condition such as the local free-stream Mach number at the leading edge. Equation (29) with equation (31) gives the result

$$\frac{p_w^{(1)}}{p_2} = 1 + \frac{\gamma G}{2} \frac{\bar{\chi}_\infty}{\left(\frac{p_2}{p_\infty}\right)^{\frac{2\gamma-1}{2\gamma}}} (1 - n)K_4 \tag{32}$$

With reference to equation (32) the following point is made; that is, by hypersonic approximation for an isentropic compression, equation (24) is

$$\frac{\bar{\chi}_\infty}{\left(\frac{p_2}{p_\infty}\right)^{\frac{2\gamma-1}{2\gamma}}} = \frac{M_2^3 \sqrt{C_2}}{\sqrt{R_2}} \equiv \bar{\chi}_2 \tag{33}$$

so that equation (28) may be written as

$$\frac{p_w^{(1)}}{p_2} = 1 + \frac{\gamma G}{2} \bar{\chi}_2 (1 - n)K_4 \tag{34}$$

Equation (34) has the same form as equation (27) and gives not too different a result even though the development of the two equations was somewhat different. Note that, with $n = 0$ and $p_2 = p_\infty$, equation (34) reduces to equation (13) (even to second order, it can be shown). Thus equation (34) is essentially the form of weak-interaction theory for self-induced effects of a boundary layer growing in a non-self-induced pressure gradient and the term $(1 - n)K_4$ is the correction term due to the external gradient.

n	$(1 - n)K_4$	
	$\gamma = 7/5$	$\gamma = 5/3$
0 0	1.000	1.000
-.1	1.119	1.104
-.2	1.237	1.208
-.3	1.364	1.313
-.4	1.502	1.421
-.5	1.649	1.533
-.6	1.801	1.648
-.7	1.965	1.769
-.8	2.145	1.895

Shown here are values of $(1 - n)K_4$ for some arbitrary values of n for favorable pressure gradients on an insulated plate in both air and helium. Other temperature ratios and values of n for air and helium or other values of γ may easily be calculated by using figure 1 and reference 1.

Weak Non-Self-Induced Pressure Gradient

It is clear that with a power-law variation of pressure with surface distance the boundary-layer growth and hence the self-induced effects depend upon the local conditions with a generally small, but not necessarily negligible, correction due to the exponent in this power-law variation of pressure. This dependence on local conditions will now be used to investigate the case where the change in local pressure, whether by external causes or changes in surface slope, is small compared to the local self-induced pressure. Based on inviscid local conditions, with the exponent in the pressure law having negligible deviation from $n = -1/2$ (the strong-interaction case), equation (17) may be written

$$\frac{p_w}{p_2} = \frac{3}{4}\sqrt{\frac{\gamma(\gamma + 1)}{2}}\, K_4 G \bar{X}_2 \tag{35}$$

where the subscript 2 indicates local inviscid conditions and the subscript w indicates surface conditions. Equation (35) written in terms of reference conditions designated by the subscript ∞ is

$$\frac{p_w}{p_\infty} = \frac{3}{4}\sqrt{\frac{\gamma(\gamma + 1)}{2}}\, K_4 G \bar{X}_\infty \left(\frac{\bar{X}_2}{\bar{X}_\infty}\frac{p_2}{p_\infty}\right) \tag{36}$$

With hypersonic flow and isentropic pressure changes, equation (33) may be applied from which

$$\frac{\bar{\chi}_2}{\bar{\chi}_\infty}\frac{p_2}{p_\infty} = \left(\frac{p_2}{p_\infty}\right)^{\frac{1}{2\gamma}} \tag{37}$$

and for small pressure deviations from the reference conditions

$$\frac{\bar{\chi}_2}{\bar{\chi}_\infty}\frac{p_2}{p_\infty} \approx 1 + \frac{1}{2\gamma}\frac{\Delta p}{p_\infty} \tag{38}$$

where $\Delta p = p_2 - p_\infty$ and, to the present approximation, equation (38) applies equally well for pressure changes caused by weak shocks. Equation (36) with equation (38) becomes

$$\frac{p_w}{p_{w,\infty}} \approx 1 + \frac{1}{2\gamma}\frac{\Delta p}{p_\infty} \approx 1 - \frac{1}{\gamma - 1}\frac{\Delta M}{M_\infty} \tag{39}$$

in which $p_{w,\infty}$ designates the strong-interaction self-induced pressure calculated for free-stream conditions which are the same as the reference conditions ∞. If the inviscid pressure change $\Delta p/p_\infty$ is due to a small surface inclination, then in terms of the hypersonic similarity parameter $K = M_\infty \omega$

$$\frac{p_w}{p_2} = 1 + \frac{K}{2} \tag{40}$$

Equations (39) and (40) allow an estimate to be made of such factors as (1) the effects of small errors in evaluating free-stream Mach number or in setting the angle of attack of a flat plate, (2) the effects of small body curvatures, and (3) the possible effects of external pressure gradients. Factors (1) and (2) are straightforwardly obtained from equations (39) and (40). Factor (3) is interesting because of the possibility of using equation (39) to evaluate the effects of longitudinal pressure gradients in conical nozzles such as those which have been used to provide much of the information on self-induced effects in helium. Data have been obtained in 1-inch- and 2-inch-diameter conical helium nozzles at Langley Research Center (refs. 7 and 14) for which the Mach number increases about 0.5 in the length of the measuring stations on a flat plate. These tests were performed at Mach numbers between 16 and 24.

In the case of Erickson's tests (ref. 14) the correlating parameters were evaluated at tunnel-empty local conditions, corresponding to the subscript 2 in the preceding development. In the investigation by Henderson and Johnston (ref. 7) the correlating parameters were evaluated at the tunnel-empty conditions at the leading edge of the model. Equation (39) indicates a difference between the two methods of evaluation of the slope of $P = P(\overline{X})$ of at most about 4 percent. Also, the $P(\overline{X})$ line from a leading-edge-condition evaluation will not pass through the $P = 1$, $\overline{X} = 0$ point.

THE BLUNTNESS-INDUCED—VISCOUS-INDUCED INTERACTION PROBLEM

Theoretical Approach

The problem of the interaction between bluntness-induced and boundary-layer-induced flow fields on a flat plate is of considerable importance. One approach to this problem is suggested by the work of Baradell and Bertram (ref. 8). In this paper, by means of the characteristics theory, surface pressure distributions on curved plates with surface coordinates given by the equation $y \propto x^m$ were investigated. It was found that addition of the pressure increment due to local plate angle (tangent-wedge theory) and the pressure increment due to the blunt leading edge (as on a flat plate) gave a result which agreed well with the characteristics theory. This blunt-leading-edge pressure-ratio contribution for $p_b/p_\infty \geqq 1.2$ is given accurately by

$$\frac{p_b}{p_\infty} = 0.187\epsilon\left[\sqrt{\gamma}(\gamma - 1)\frac{M_\infty^3 k}{x/t}\right]^{2/3} + 0.74 \tag{41}$$

where ϵ is a small correction term to the function of γ shown above which can be represented by $\epsilon \approx 1 - \left[0.0048/(\gamma - 1)^2\right]$. Equation (41) is found to give good results from constant γ of 6/5 to 9/5 based on the results in reference 8.

The curved plate in the problem of reference 8 is replaced by the displacement thickness of the boundary layer. The growth of this boundary layer is assumed to be controlled by the pressures on the plate and by the undisturbed free-stream Mach number; that is, no account is taken of the entropy jump at the leading edge. The decrease in Mach number associated with the leading-edge entropy jump is assumed to be compensated for by the decrease in Reynolds number.

Two different cases for the problem of surface pressures induced by blunt-leading-edge viscous interaction will be shown. In the first case

the blunt-leading-edge-induced pressures are assumed to be large compared with the viscous-induced increment in pressure. In the second case the viscous-induced increment in pressure is too large to be ignored and contributes significantly to the induced effect on boundary-layer growth. If the blunt-leading-edge-induced pressures are assumed to be large compared with free-stream pressure and much larger than the viscous-induced increment, then the slope of the edge of the boundary layer in hypersonic similarity form may be given by equation (20) in the following form ($n = -2/3$ from eq. (41)):

$$K_\delta \equiv M_\infty \delta_x' = \frac{5}{6} \frac{K_4 G \bar{X}_\infty}{\sqrt{p_b/p_\infty}} \tag{42}$$

Taking the coefficient K_4 as unity (see fig. 1) and substituting equation (42) into the first-order form of equation (10) to represent the tangent-wedge portion of the solution yields

$$\frac{\Delta p_v^{(1)}}{p_\infty} = \frac{5}{6} \frac{\gamma G \bar{X}_\infty}{\sqrt{p_b/p_\infty}} \tag{43}$$

or to the second order

$$\frac{\Delta p_v^{(2)}}{p_\infty} = \frac{\Delta p_v^{(1)}}{p_\infty} + \frac{\gamma + 1}{4\gamma} \left(\frac{\Delta p_v^{(1)}}{p_\infty} \right)^2 \tag{44}$$

The parameter that controls the blunt-leading-edge-induced pressure in equation (41) may be written as follows:

$$\frac{M_\infty^3 k}{x/t} \equiv \frac{k R_t \bar{X}_\infty^{-2}}{M_\infty^3 C} \tag{45}$$

Thus for a given value $kR_t/M_\infty^3 C$ the wall pressure $\left(p_w = p_b + \Delta p_v\right)$ is a function of $\bar{X}_\infty$ only. This result can be obtained from reference 15 which uses a considerably different development.

In the second case, the effect of the viscous-induced pressure increment on the boundary-layer growth must be accounted for. In this case, equation (20) is written as

$$K_\delta = \frac{(1 - n)K_4}{2} \frac{G\bar{X}_\infty}{\sqrt{\frac{p_b}{p_\infty} + \frac{\Delta p_v}{p_\infty}}} \tag{46}$$

The form of equation (15) for large values of K_δ is taken as $\frac{\Delta p_v}{p_\infty} = \left[\frac{\gamma(\gamma + 1)}{2}\right] K_\delta^2$ and when this equation is substituted in equation (46) the solution is

$$\frac{\Delta p_v}{p_\infty} = \frac{1}{2}\left\{\sqrt{\left(\frac{p_b}{p_\infty}\right)^2 + \frac{\gamma(\gamma + 1)}{2}\left[(1 - n)K_4\right]^2 \left(G\bar{X}_\infty\right)^2} - \frac{p_b}{p_\infty}\right\} \tag{47}$$

Comparison With Experiment

In order to check these predictions of viscid-inviscid interaction effects figures 7 and 8 have been prepared which show much of the data available on flat plates in air and helium. In figure 7 data obtained on essentially insulated flat-leading-edge plates in helium from references 7, 14, 16, and 17 plus some new data obtained in the Langley 11-inch hypersonic tunnel (see appendix) have been put into groups with approximately the same value of $kR_t/M_\infty^3 C$. First it may be noted that there appears, in general, to be good correlation of the data for given values of the parameter $kR_t/M_\infty^3 C$. Some random deviations from correlation may be noted; however, these deviations do not appear to be associated with any particular Mach number or Reynolds number trend. The sort of deviation or scatter referred to is illustrated in figures 7(b) and 7(c) by the data obtained by Henderson and Johnston (ref. 7) for values of $kR_t/M_\infty^3 C$ of about 5 (square symbols) and 6.6 (diamond symbols). These sets of data (compare flagged and unflagged symbols) were obtained under almost the same conditions.

The strong viscid-inviscid interaction theory (eq. (47)) does a good job of predicting the surface pressures except perhaps at values of $kR_t/M_\infty^3 C$ below about 1.5 where the pure viscous theory appears to be preferable. At values of $kR_t/M_\infty^3 C$ where inviscid effects are dominant (above about 14) the first-order weak viscid-inviscid interaction theory (eq. (43)) gives much the same answer as equation (41) and both agree well with the data.

Much the same result is obtained for the data available in air flows shown in figure 8. The data (refs. 17 to 22 plus new data obtained in the Langley 11-inch hypersonic tunnel), in general, show good agreement with the theories. It should be noted that, although for the data presented in figure 7 the lowest value of kR_t/M_∞^3C is about 4, the data presented in figure 6 for comparison with pure viscous theory had very much lower values of kR_t/M_∞^3C, values which varied from 0.15 to 0.5 for the $M = 5.8$ data (ref. 10) and from 0.05 to 0.1 for the $M = 9.6$ data of the present tests.

There are, however, some cases where there is a major disagreement between experiment and theory. This disagreement generally occurs for data obtained in the region close to the leading edge. Data obtained in approximately the first two diameters from the leading edge in figure 8 are indicated by the filled symbols which generally correspond to the data showing the large disagreement. It is in this region close to the leading edge that the effect of nose shape is important in determining the pressure distribution.

Analysis of data in the near-leading-edge region, however, can also be complicated by low-density effects. This is illustrated in figure 9 by data obtained in the University of California low density tunnel by Aroesty (ref. 23) at $M \approx 3.9$ and by Schaaf, Hurlbut, and Talbot (ref. 18) at $M \approx 5.7$. Aroesty's data (fig. 9(a)) were obtained at very low Knudsen numbers for the leading-edge thickness and shows qualitatively the same slope pattern at the larger values of $\overline{X}$ as is shown in the pressures measured by Schaaf, Hurlbut, and Talbot (fig. 9(b)) at Knudsen numbers which ranged from relatively high (2.1) to quite low (0.01). Figure 10 can be used to illustrate that this rather similar behavior of the data from reference 18 for the widely different Knudsen numbers is fortuitous. In figure 10 the pressure data of reference 18 are plotted against x/t rather than against the parameter $\overline{X}$ for the first 10 diameters downstream of the leading edge of the plate. Shown also for comparison purposes are Creager's essentially inviscid data (ref. 20) obtained at a relatively high density on a flat-leading-edge plate. Note that except for the magnitude the shape formed by the University of California data for the lower Knudsen numbers $\left(N_{Kn} \leqq 0.04\right)$ is much the same as that of Creager's. The University of California data at the higher Knudsen numbers $\left(N_{Kn}\right.$ of 0.1 and 0.2$\left.\right)$ is not data from the near-leading-edge region and only coincidentally has roughly the same level of pressure as the data from the first two or three diameters at the lower Knudsen numbers. This fortuity is further corroborated by the fact that even though Aroesty and Creager obtained their data at about the same Mach numbers the maximum pressure ratio obtained by Creager is about 2 (fig. 10) but by Aroesty is about 3.5 (fig. 9(a)).

Oguchi has considered the problem of the prediction of the viscous-induced pressures in this near-leading-edge region (ref. 24). By utilizing a wedge-like boundary-layer growth in this region, apparently he has obtained a solution which successfully predicts the pressure levels obtained at low densities in references 23 and 25.

Extension to the Case of Blunt-Nosed Rods

Equations (43) and (47) may be written in terms of the inviscid parameters for both flat plates and rods if for the rod the boundary layer is not too thick compared with the radius of the rod and results are obtained far enough back of the nose so that the three dimensionality of the nose is not important. For example, if the nose of the rod has a hemispherical shape then the number of diameters downstream from the nose must be large compared with $\pi/8$ (ref. 1).

This more general form of equation (43) is

$$\frac{\Delta p_v^{(1)}}{p_\infty} = \frac{5}{6}\gamma \frac{G}{\sqrt{\dfrac{k^{\frac{1}{1+j}} R_t}{M_\infty^{3+j} C}}} \left(\frac{\dfrac{M_\infty^{3-j} k^{\frac{1}{1+j}}}{x/t}}{\dfrac{p_b}{p_\infty}} \right)^{1/2} \tag{48}$$

and of equation (47) is

$$\frac{\Delta p_v}{p_\infty} = \frac{1}{2}\left[\sqrt{\left(\frac{p_b}{p_\infty}\right)^2 + \frac{\gamma(\gamma+1)}{2}\left[(1-n)K_4\right]^2 \left(\frac{G}{\sqrt{\dfrac{k^{\frac{1}{1+j}} R_t}{M_\infty^{3+j} C}}} \right)^2 \frac{M_\infty^{3-j} k^{\frac{1}{1+j}}}{x/t}} - \frac{p_b}{p_\infty} \right] \tag{49}$$

in which $j = 0$ for the planar case and $j = 1$ for the rod alined with flow (see eq. (5) of ref. 8). The symbol t represents the leading-edge thickness in the two-dimensional case and the diameter of the rod in the cylindrical case.

Calculations based on equation (49) are presented in figures 11 and 12 for air and helium. Figure 11 shows results for the two-dimensional case utilizing equation (49) with equation (41). The solid line is the inviscid case given directly by equation (41). The increments between the solid curve and the dashed curves represent the viscous-induced pressure increments predicted by equation (49). The parameter G (eq. (3)

or eq. (14)) takes into account the wall temperature level. In computations for figure 11, the value of n in equation (49) was taken as constant at a value of 0.6. The error that this introduces can be assessed by noting that the local value of n is the local slope of the curves in figure 11.

To generalize from the experimental insulated-plate results presented previously and compared to equations (48) and (49) (or to their less general forms - equations (43) and (47)), consider values of the parameter $G\Big/\sqrt{kR_t\Big/M_\infty^3 C}$. When the value of this parameter is greater than about 2/3, the effects of leading-edge bluntness are virtually negligible. When the value of this parameter is less than about 1/2, blunt-leading-edge-induced pressure effects are important and the theory developed in this paper gives a good prediction of the surface pressures. For values of the correlation parameter less than about 1/10 the viscous-induced contribution is small to negligible compared with the contribution of the blunt leading edge to the surface pressures.

An analogous presentation is made for the blunt rod in figure 12. In this case equation (49) was used with an empirical equation obtained by Van Hise (ref. 26) based on characteristics solutions for rods with various bluntnesses. This equation is

$$\frac{p_b}{p_\infty} = \xi\frac{M_\infty^2\sqrt{k}}{x/d} + 0.55 \tag{50}$$

in which $\xi = 0.060$ for $\gamma = 7/5$ and $\xi = 0.075$ for $\gamma = 5/3$. The solid line in figure 12 is the inviscid case given by equation (50). Again the increments between the solid curve and the dashed curves represent the viscous-induced pressure increments predicted by equation (49). In computations for figure 12, the value of n in equation (49) was taken as that given by equation (50). (See discussion before eq. (9).) This introduces some error since, judging from the computed curves, the value of n for the case with viscous interaction will always be less than the value of n given by equation (50). In figure 12, d has been used to represent the t in equation (49) as in equation (50).

CONCLUDING REMARKS

This paper has shown the simplified theoretical approaches, based on hypersonic similarity boundary-layer theory, presently available which allow reasonably accurate estimates to be made of the surface

pressures on plates on which viscous effects are important. The consideration of viscous effects includes the cases where curved surfaces, stream pressure gradients, and leading-edge bluntness are important factors.

In a simple attack on the problem of the effect on the surface pressure of the interaction between flow fields induced by leading-edge blunting and boundary-layer displacement effects, equations have been derived which in general give a good prediction of the surface pressures. The parameter determining the level of the surface pressure induced on a two-dimensional flat plate by the interaction of blunt-leading-edge-induced and boundary-layer-induced flow fields was found to be $G\sqrt{\sqrt{kR_t}/M_\infty^3 C}$ where G is a wall temperature and Mach number function in the laminar-boundary-layer growth equation, k is the nose drag coefficient, R_t is the Reynolds number based on leading-edge thickness, M_∞ is the free-stream Mach number, and C is the coefficient in the linear viscosity law. Correlations of the available data according to this parameter indicate the effects of leading-edge bluntness are virtually negligible when the value of this parameter is greater than about 2/3. When the value of this parameter is less than about 1/2, blunt-leading-edge-induced pressure effects are important and the theory developed in this paper gives a good prediction of the surface pressures. For values of the correlation parameter less than about 1/10 the viscous-induced contribution is small to negligible compared with the contribution of the blunt leading edge to the surface pressure.

An extension of the theory to the case of the blunt-nosed rod alined with the free-stream flow also allows a prediction of the surface pressure induced by viscid-inviscid interaction for this special three-dimensional case.

Langley Research Center,
National Aeronautics and Space Administration,
Langley Field, Va., February 9, 1961.

APPENDIX

DESCRIPTION OF NOZZLES AND MODEL USED TO OBTAIN DATA IN THE LANGLEY 11-INCH HYPERSONIC TUNNEL

Tunnel and Nozzles

The unpublished data shown in this report were obtained from tests conducted in the Langley 11-inch hypersonic tunnel. The Mach number of this blowdown facility can be varied by changing nozzles. In the present tests, nozzles giving nominal Mach numbers of 6.8 and 9.6 with air and 18 with helium were used. The Mach number 6.8 air nozzle is a contoured two-dimensional nozzle machined from Invar to minimize deflection of the nozzle throat due to thermal gradients. A calibration of this nozzle may be found in reference 27. The Mach number 9.6 nozzle is a contoured three-dimensional nozzle with square throat and test section. The calibration for this nozzle is given in reference 2. The Mach number 18 helium nozzle is contoured to obtain uniform flow and has a circular cross section. A complete description and calibration of this nozzle and other helium nozzles used at the Langley 11-inch hypersonic tunnel may be found in references 28 and 29.

Models and Instrumentation

The model used in this investigation is the slab wing with the various leading edges shown in figure 13. The 36° wedge leading edge was designed to give sonic velocity behind the shock at Mach number 18 in helium and the 43° wedge leading edge was designed to give approximately sonic velocity behind the shock at Mach numbers of 6.8 and 9.6 in air. Surface pressures were measured by means of the aneroid-type six-cell recording units described in reference 30. The skin temperatures were obtained from chromel-alumel thermocouples formed from No. 30 wire. The thermocouple wires were spotwelded to the underside of the surface and the skin temperatures were recorded on self-balancing potentiometers. Some typical wall-temperature distributions are shown in figure 14. These temperature distributions are ones obtained with the 0.060-inch-thick flat-face leading edge; however, they are representative of the distributions obtained for all of the various leading edges. For the nominal Mach number 6.8 tests, temperature distributions are shown for two different Reynolds numbers. For the tests at Mach numbers of 9.6 and 18 the effect of Reynolds number on the temperature distribution was small and only one distribution for these Mach numbers is shown.

REFERENCES

1. Bertram, Mitchel H., and Feller, William V.: A Simple Method for Determining Heat Transfer, Skin Friction, and Boundary-Layer Thickness for Hypersonic Laminar Boundary-Layer Flows in a Pressure Gradient. NASA MEMO 5-24-59L, 1959.

2. Bertram, Mitchel H.: Boundary-Layer Displacement Effects in Air at Mach Numbers of 6.8 and 9.6. NASA TR R-22, 1959. (Supersedes NACA TN 4133.)

3. Beckwith, Ivan E., and Cohen, Nathaniel B.: Application of Similar Solutions to Calculation of Laminar Heat Transfer on Bodies With Yaw and Large Pressure Gradient in High-Speed Flow. NASA TN D-625, 1961.

4. Lees, Lester: Hypersonic Flow. Fifth International Aeronautical Conference (Los Angeles, Calif., June 20-23, 1955), Inst. Aero. Sci., Inc., 1955, pp. 241-276.

5. Lees, Lester, and Probstein, Ronald F.: Hypersonic Viscous Flow Over a Flat Plate. Rep. no. 195 (Contract AF 33(038)-250), Aero. Eng. Lab., Princeton Univ., Apr. 20, 1952.

6. Probstein, Ronald F.: Interacting Hypersonic Laminar Boundary Layer Flow Over a Cone. Tech. Rep. AF 2798/1 (Contract AF 33(616)-2798), Div. Eng., Brown Univ., Mar. 1955.

7. Henderson, Arthur, Jr., and Johnston, Patrick J.: Fluid-Dynamic Properties of Some Simple Sharp- and Blunt-Nosed Shapes at Mach Numbers From 16 to 24 in Helium Flow. NASA MEMO 5-8-59L, 1959.

8. Baradell, Donald L., and Bertram, Mitchel H.: The Blunt Plate in Hypersonic Flow. NASA TN D-408, 1960.

9. Chernyi, G. G.: Effect of Slight Blunting of Leading Edge of an Immersed Body on the Flow Around It at Hypersonic Speeds. NASA TT F-35, 1960. (From Izvestiia Otd. Tekh. Nauk (An USSR), no. 4, Apr. 1958, pp. 54-66.)

10. Kendall, James M., Jr.: An Experimental Investigation of Leading-Edge Shock-Wave - Boundary-Layer Interaction at Mach 5.8. Jour. Aero. Sci., vol. 24, no. 1, Jan. 1957, pp. 47-56.

11. Bertram, Mitchel H., and Henderson, Arthur, Jr.: Effects of Boundary-Layer Displacement and Leading-Edge Bluntness on Pressure Distribution, Skin Friction, and Heat Transfer of Bodies at Hypersonic Speeds. NACA TN 4301, 1958.

12. Dryden, Hugh L.: Gegenwartsprobleme der Luftfahrtforschung. Zs. f. Flugwissenschaften, Jahrg. 6, Heft 8, Aug. 1958, pp. 217-233.

13. Hayes, Wallace D., and Probstein, Ronald F.: Hypersonic Flow Theory. Academic Press, Inc. (New York), 1959, pp. 333-374.

14. Erickson, Wayne D.: Study of Pressure Distributions on Simple Sharp-Nosed Models at Mach Numbers From 16 to 18 in Helium Flow. NACA TN 4113, 1957.

15. Cheng, H. K., Hall, J. Gordon, Golian, T. C., and Hertzberg, A.: Boundary-Layer Displacement and Leading-Edge Bluntness Effects in High-Temperature Hypersonic Flow. Paper no. 60-38, Inst. Aero. Sci., Jan. 1960.

16. Vas, Irwin E.: An Experimental Investigation of the Pressure on a Thin Flat Plate at Hypersonic Speeds. Rep. no. 377 (WADC TN 57-104, AD 118151), Dept. Aero. Eng., Princeton Univ., Mar. 1957.

17. Bertram, Mitchel H., and Henderson, Arthur, Jr.: Recent Hypersonic Studies of Wings and Bodies. [Preprint] 1131-60, Am. Rocket Soc., May 1960.

18. Schaaf, S. A., Hurlbut, F. C., and Talbot, L.: Induced Pressures on Flat Plates in Hypersonic Low Density Flow. ARDC TR 57-47 (AD 113 008), U.S. Air Force, Jan. 25, 1957.

19. Bertram, Mitchel H.: Viscous and Leading-Edge Thickness Effects on the Pressures on the Surface of a Flat Plate in Hypersonic Flow. Jour. Aero. Sci. (Readers' Forum), vol. 21, no. 6, June 1954, pp. 430-431.

20. Creager, Marcus O.: Effects of Leading-Edge Blunting on the Local Heat Transfer and Pressure Distributions Over Flat Plates in Supersonic Flow. NACA TN 4142, 1957.

21. Creager, Marcus O.: The Effect of Leading-Edge Sweep and Surface Inclination on the Hypersonic Flow Field Over a Blunt Flat Plate. NASA MEMO 12-26-58A, 1959.

22. Kim, Chul-Soo: Experimental Studies on the Hypersonic Flow Past Plane, Convex and Concave Wedges. Jour. Phys. Soc. of Japan, vol. 14, no. 6, June 1959, pp. 827-837.

23. Aroesty, Jerome: Pressure Distributions on Flat Plates at Mach 4 and Low Density Flow. Rep. no. HE-150-157 (Ser. 20-120, Contract N-onr-222(45)), Inst. Eng. Res., Univ. of California, July 28, 1958.

24. Oguchi, Hakuro: The Sharp Leading Edge Problem in Hypersonic Flow. ARL TN 60-133 (Contract no. AF 33(616)-5442), Div. Eng., Brown Univ., Aug. 1960.

25. Nagamatsu, H. T., Sheer, R. E., Jr., and Schmid, J. R.: High Temperature Rarefied Ultra-High Mach Number Flow Over a Flat Plate. [Preprint] 1132-60, Am. Rocket Soc., May 1960.

26. Van Hise, Vernon: Analytic Study of Induced Pressure on Long Bodies of Revolution With Varying Nose Bluntness at Hypersonic Speeds. NASA TR R-78, 1961.

27. Bertram, Mitchel H.: Exploratory Investigation of Boundary-Layer Transition on a Hollow Cylinder at a Mach Number of 6.9. NACA Rep. 1313, 1957. (Supersedes NACA TN 3546.)

28. Armstrong, William O., and Ladson, Charles L. (With Appendix A by Donald L. Baradell and Thomas A. Blackstock): Effects of Variation in Body Orientation and Wing and Body Geometry on Lift-Drag Characteristics of a Series of Wing-Body Combinations at Mach Numbers From 3 to 18. NASA TM X-73, 1959.

29. Henderson, Arthur, Jr., and Baradell, Donald L.: Recent Work at Langley Research Center in the Development of Hypersonic Helium Tunnels. Proc. Nat. Symposium on Hypervelocity Techniques (Denver, Colo.), Inst. Aero. Sci., Oct. 20-21, 1960, pp. 131-141.

30. McLellan, Charles H., Williams, Thomas W., and Bertram, Mitchel H.: Investigation of a Two-Step Nozzle in the Langley 11-Inch Hypersonic Tunnel. NACA TN 2171, 1950.

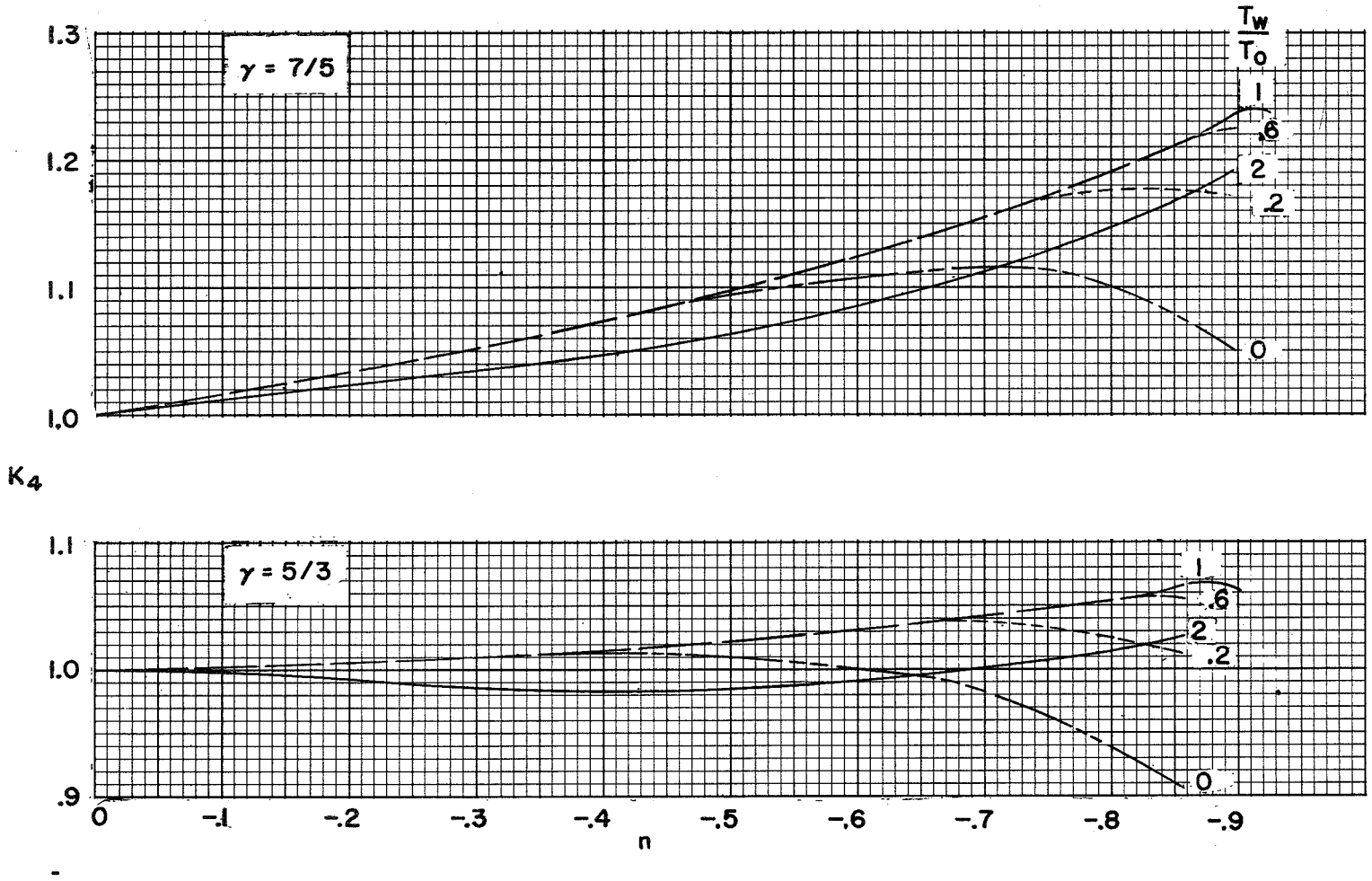

Figure 1.- Variation of coefficient in hypersonic similarity boundary-layer-thickness law with pressure gradient.

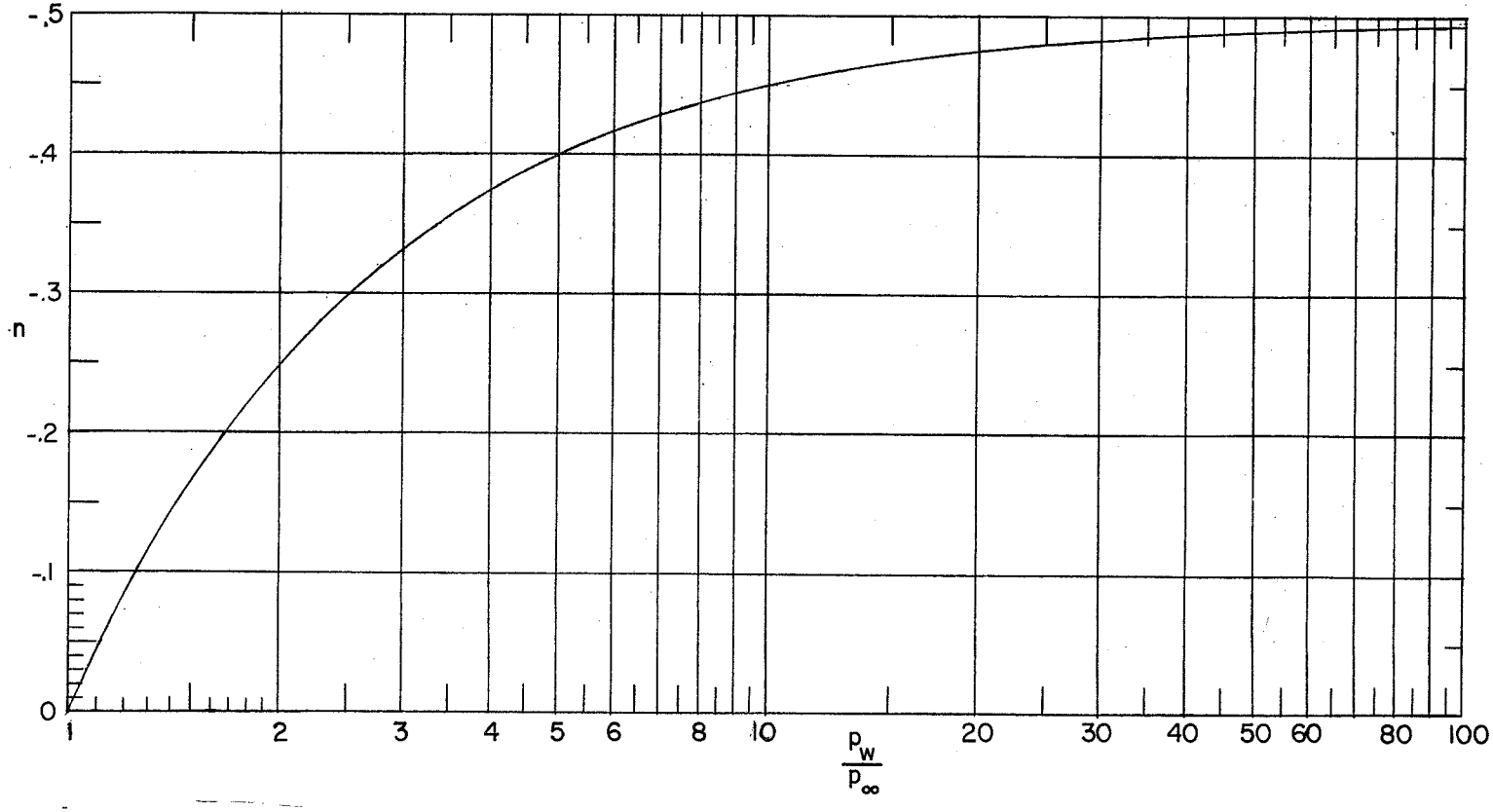

Figure 2.- Variation of exponent n in power law $\frac{p_w}{p_\infty} = 1 + ax^{-\frac{1}{2}} = x^n$.

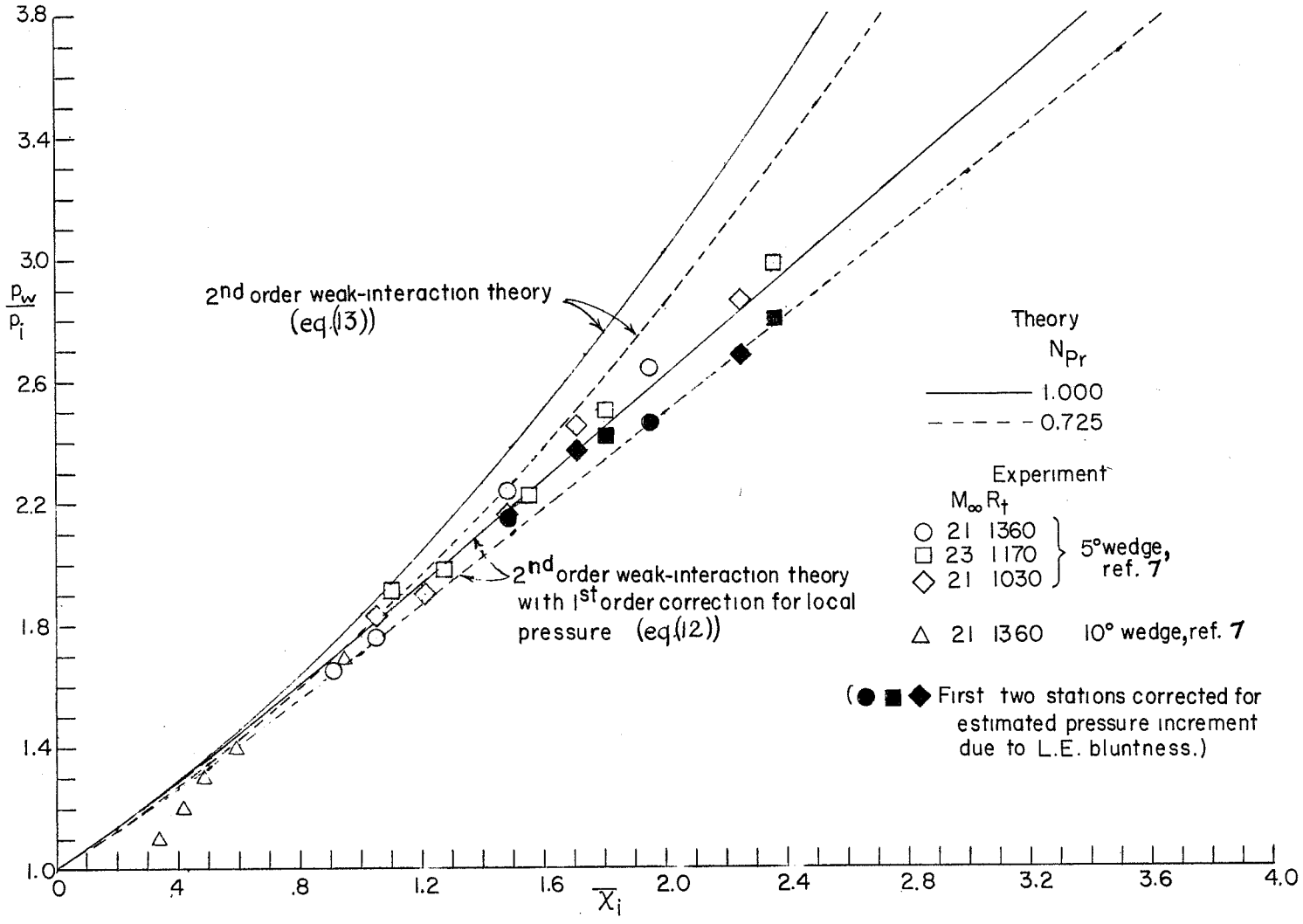

Figure 3.- Comparison of theory with experiment on an insulated flat plate in helium for weak-interaction theory and a higher order approximation.

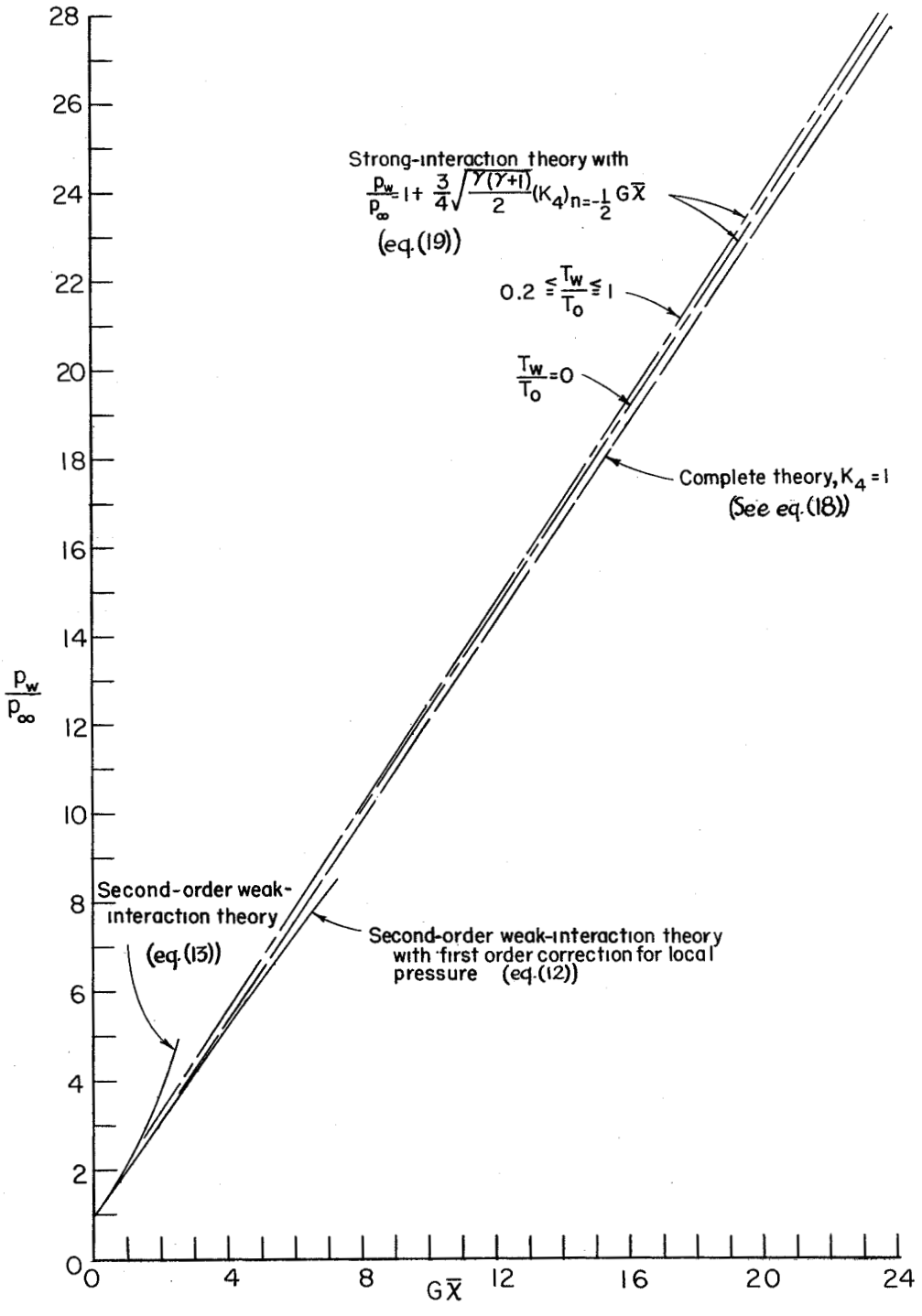

Figure 4.- Comparison of various theories for predicting boundary-layer displacement effects on a flat plate. $\gamma = 5/3$; $N_{Pr} = 1$.

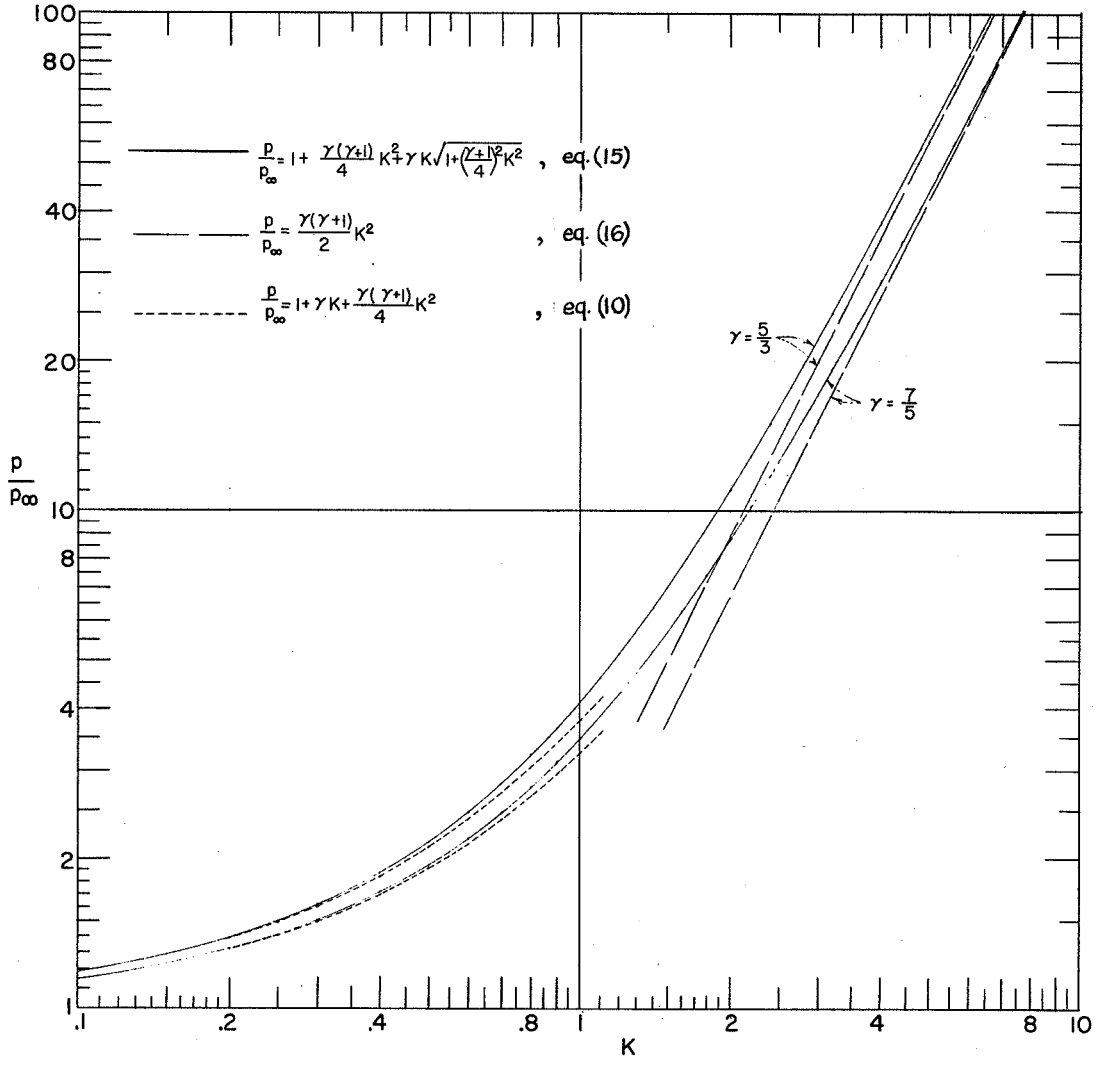

Figure 5.- Static-pressure ratio across oblique shock as a function of the similarity deflection angle according to hypersonic similarity theory.

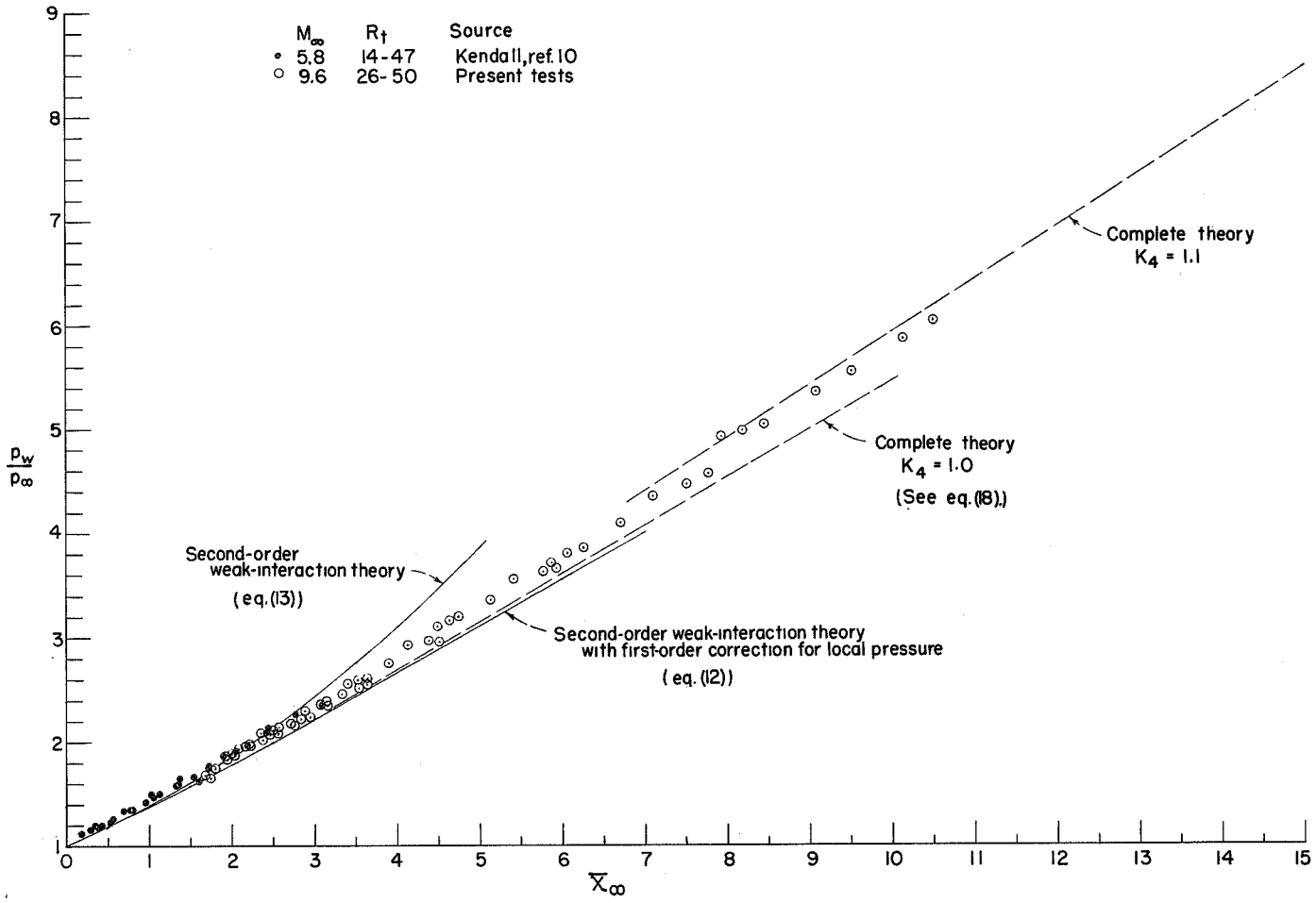

(a) $\alpha = 0$.

Figure 6.- Various theories for predicting boundary-layer displacement effects on a flat plate in air and comparison with experiment.

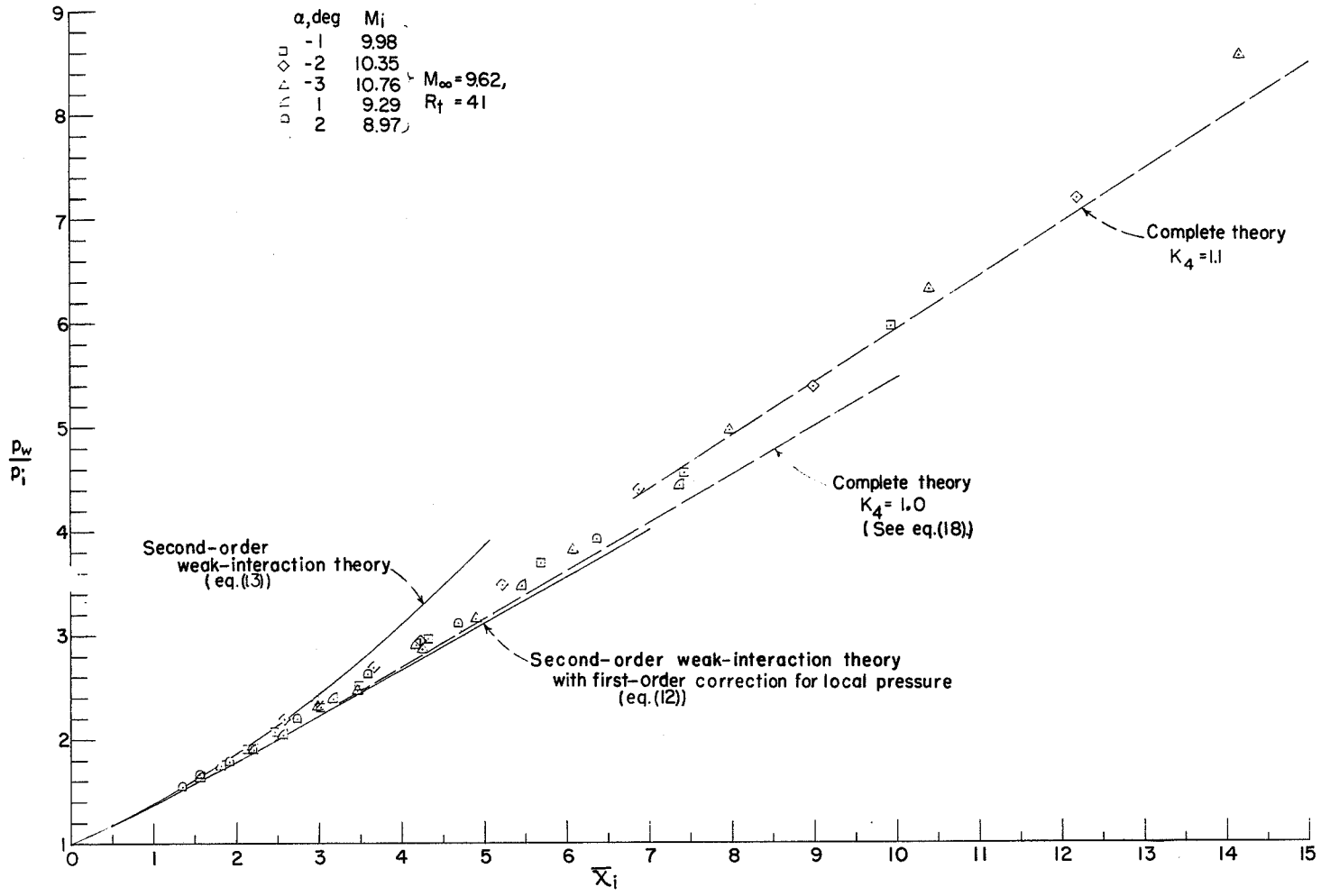

(b) $\alpha \neq 0$.

Figure 6.- Concluded.

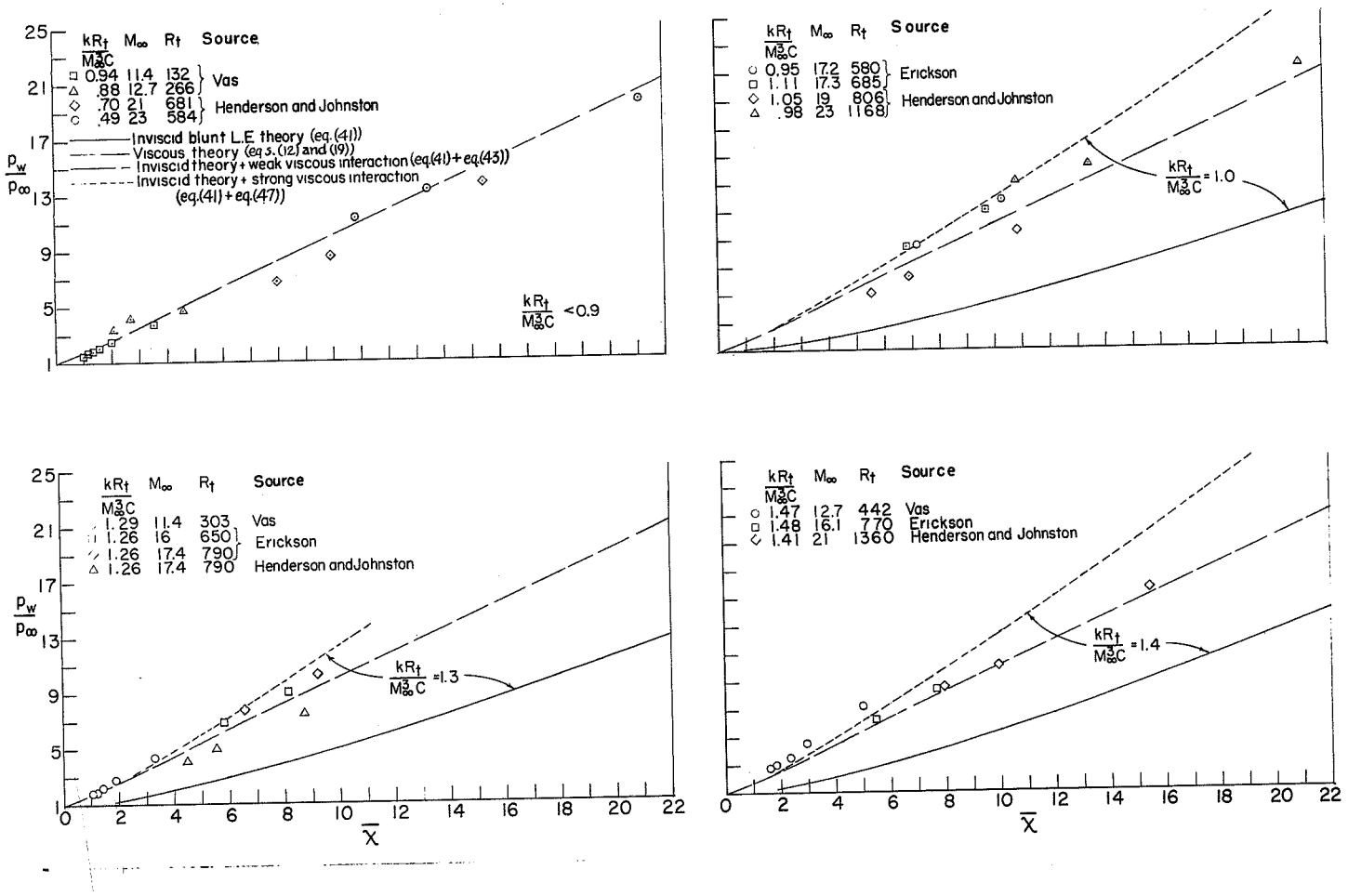

(a) $\frac{kR_t}{M_\infty^3 C}$ in range from about 0.5 to about 1.5.

Figure 7.- Correlation of induced pressures in helium and comparison of theory with experiment. Insulated flat plate with flat leading edge at $\alpha = 0$.

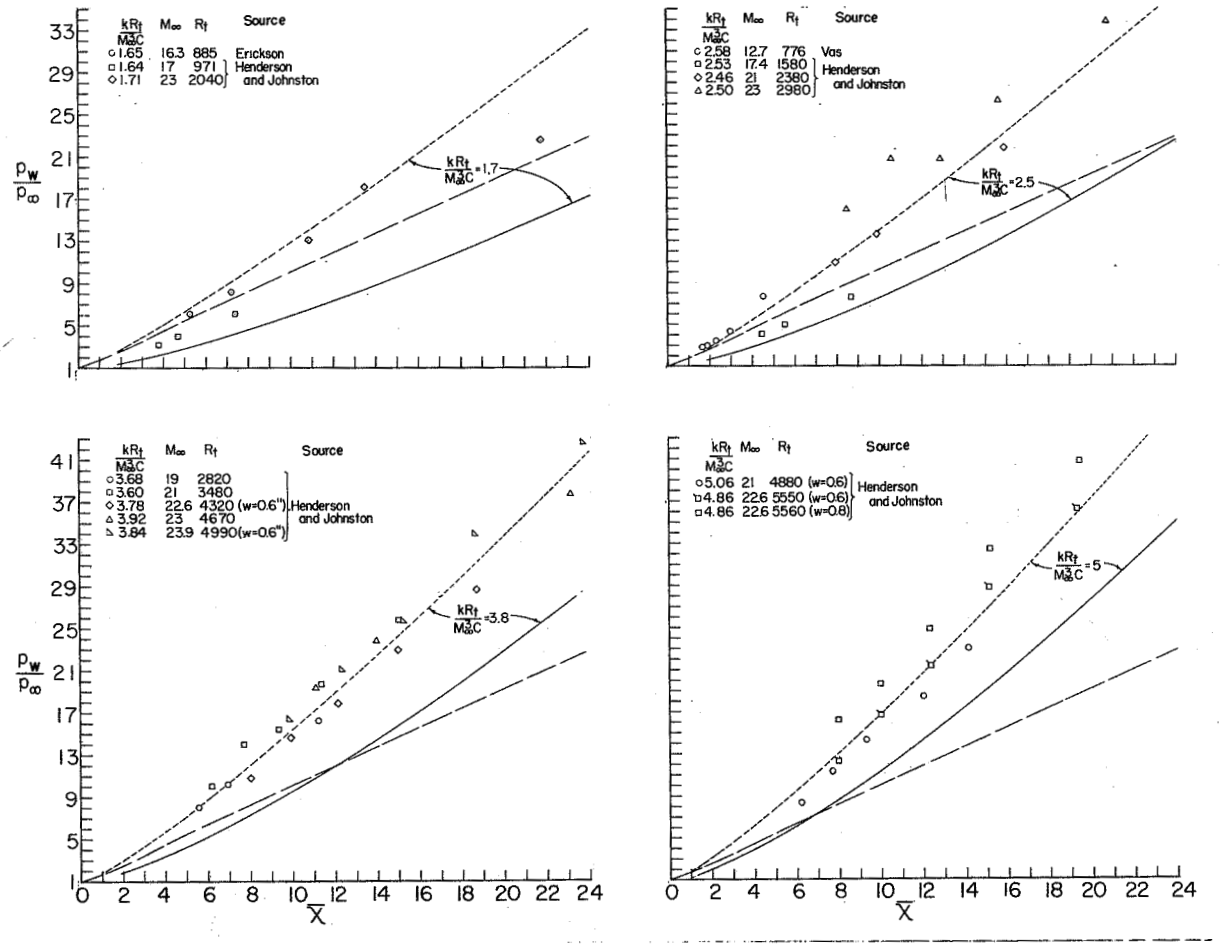

(b) $\frac{kR_t}{M_\infty{}^3C}$ in range from about 1.7 to about 5.

Figure 7.- Continued.

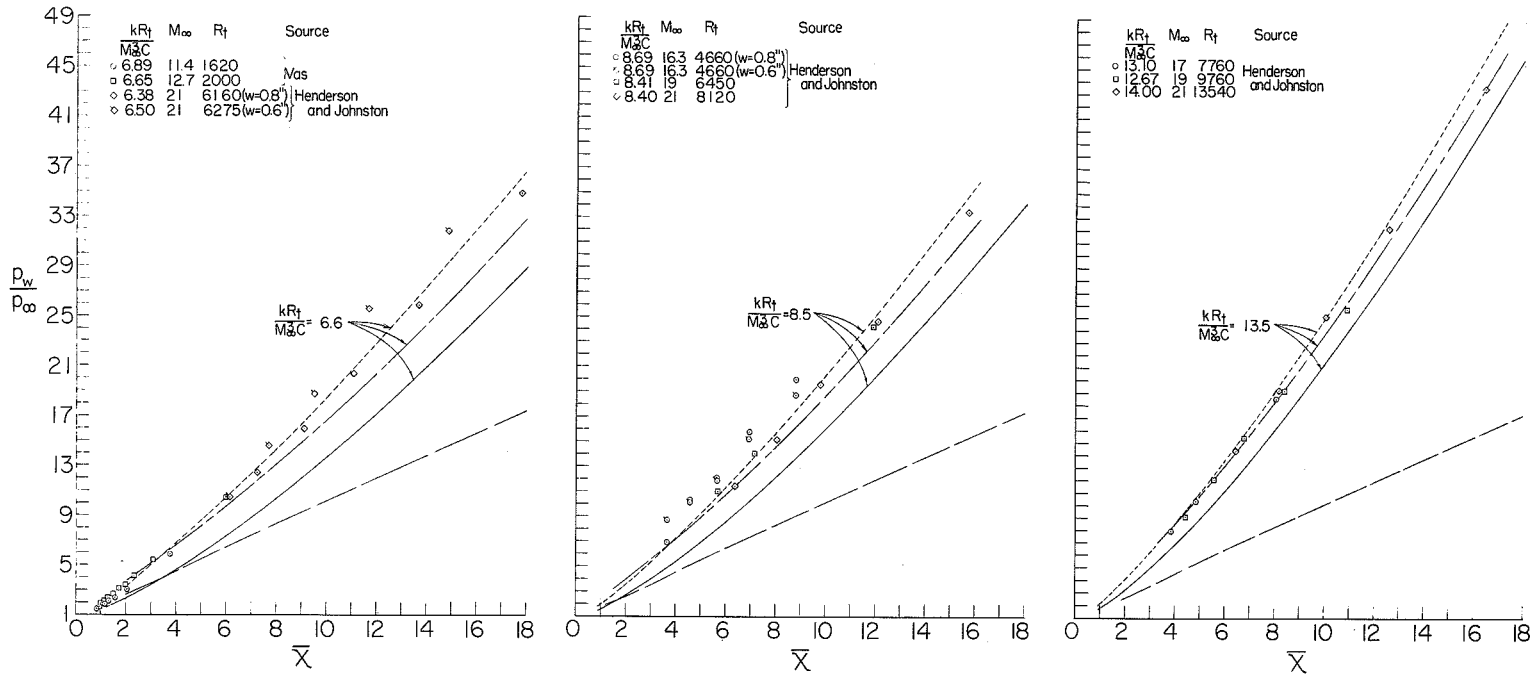

(c) $\frac{kR_t}{M_\infty{}^3C}$ in range from about 6 to about 14.

Figure 7.- Continued.

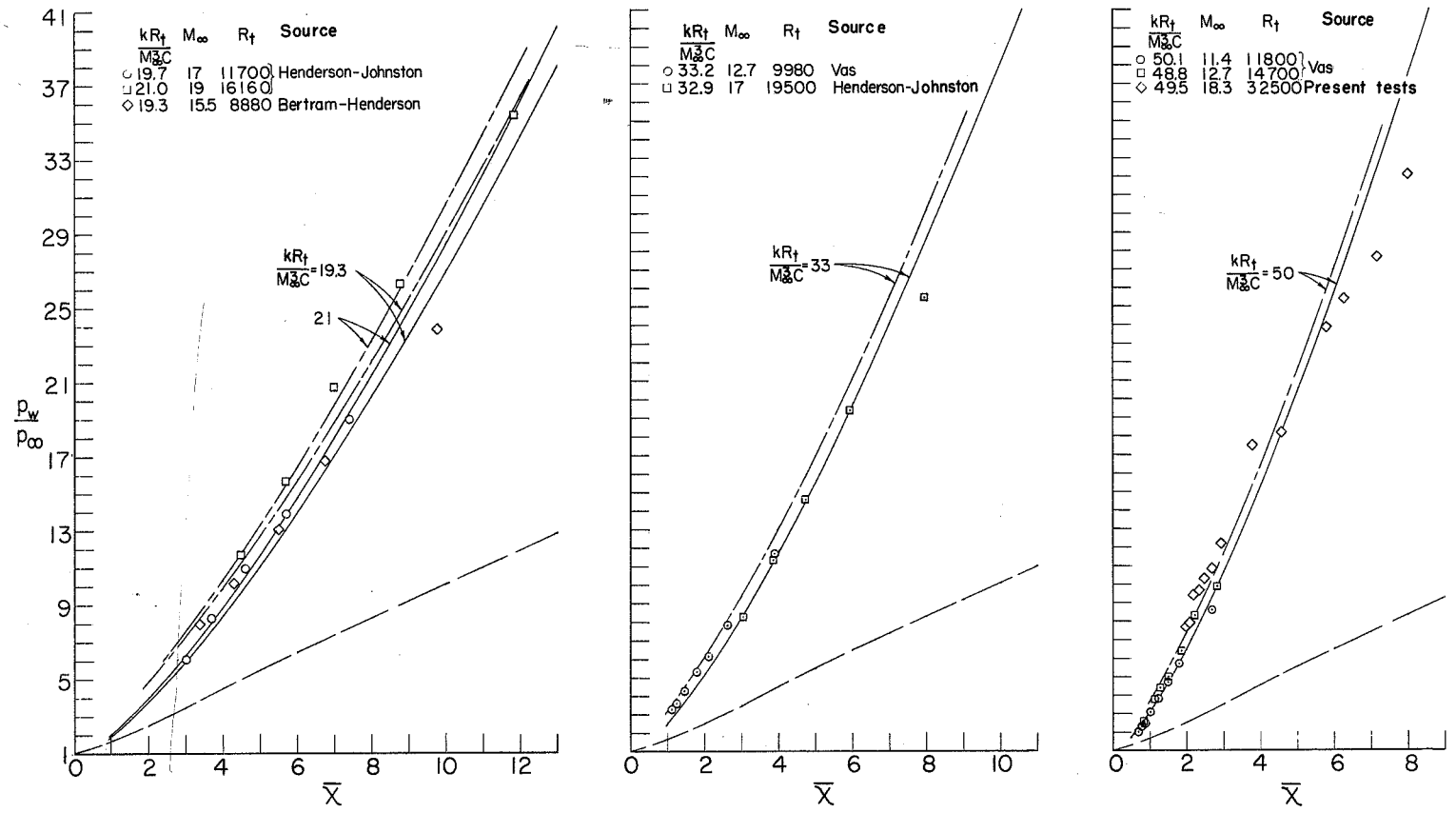

(d) $\frac{kR_t}{M_\infty{}^3C}$ in range from about 19 to about 50.

Figure 7.- Concluded.

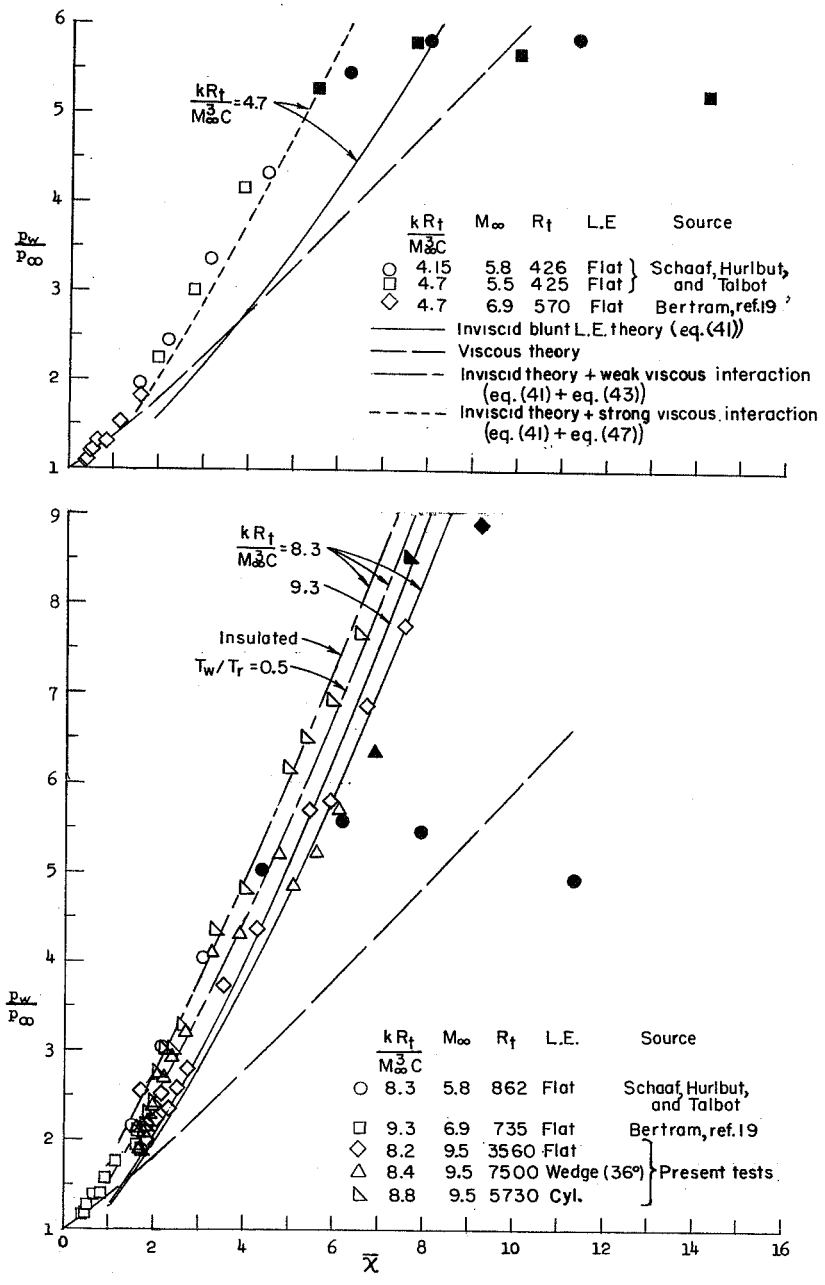

(a) $\frac{kR_t}{M_\infty^3 C}$ in range from about 4 to about 9.

Figure 8.- Correlation of induced pressures on flat plate in air and comparison of theory with experiment. Solid symbols indicate data obtained two diameters or less from leading edge.

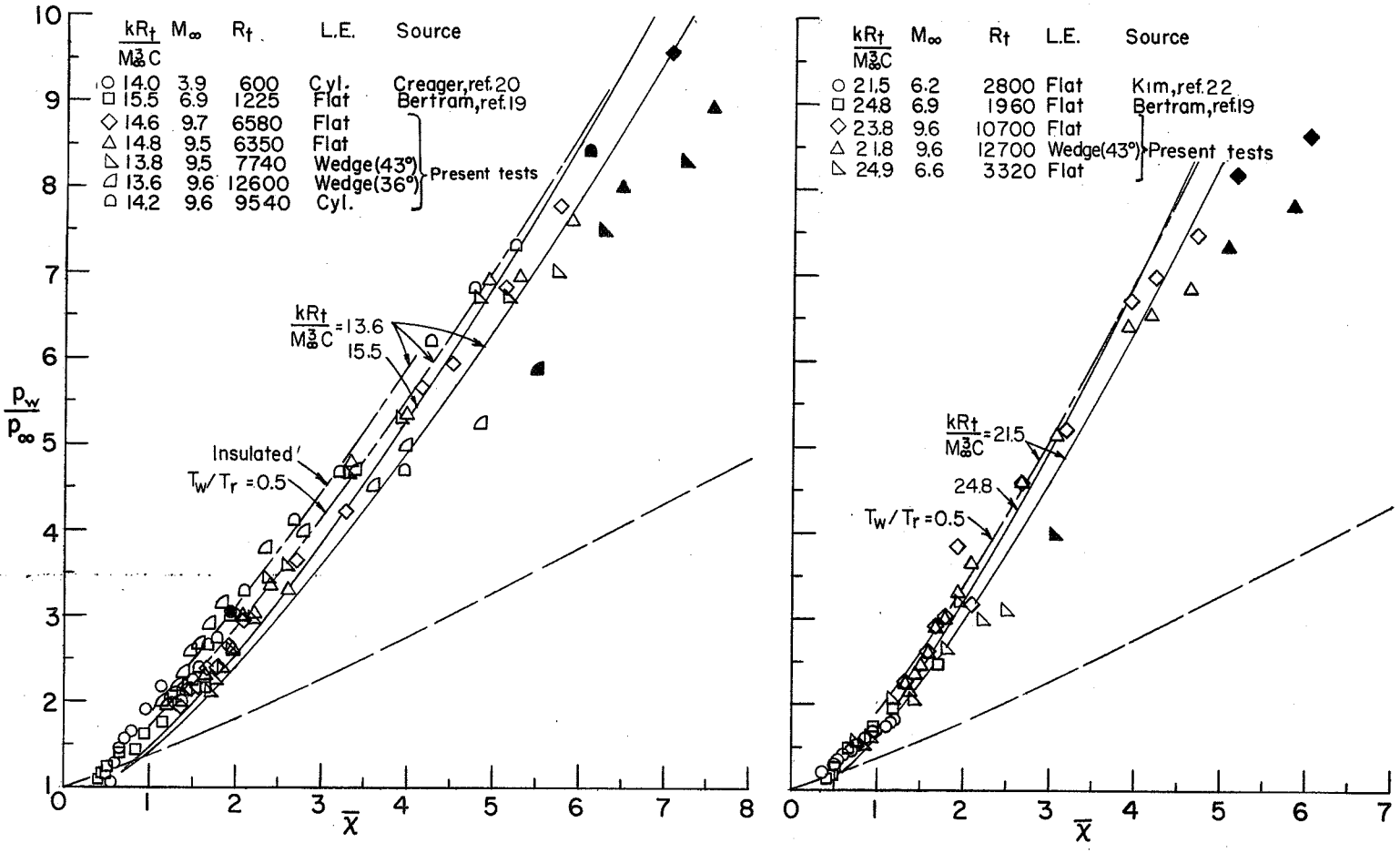

(b) $\frac{kR_t}{M_\infty{}^3C}$ in range from about 14 to about 24.

Figure 8.- Continued.

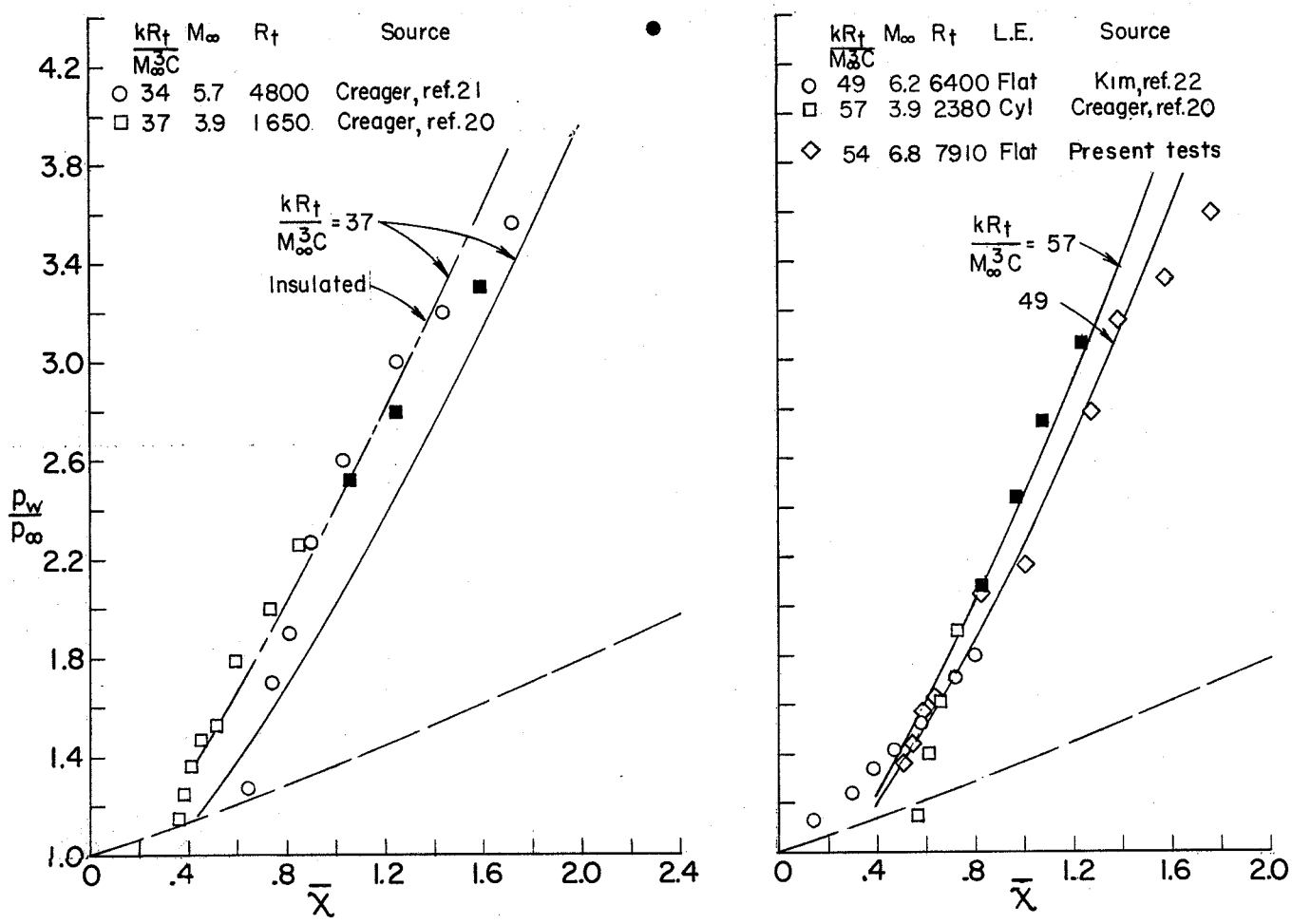

(c) $\frac{kR_t}{M_\infty{}^3C}$ in range from about 34 to about 57.

Figure 8.- Continued.

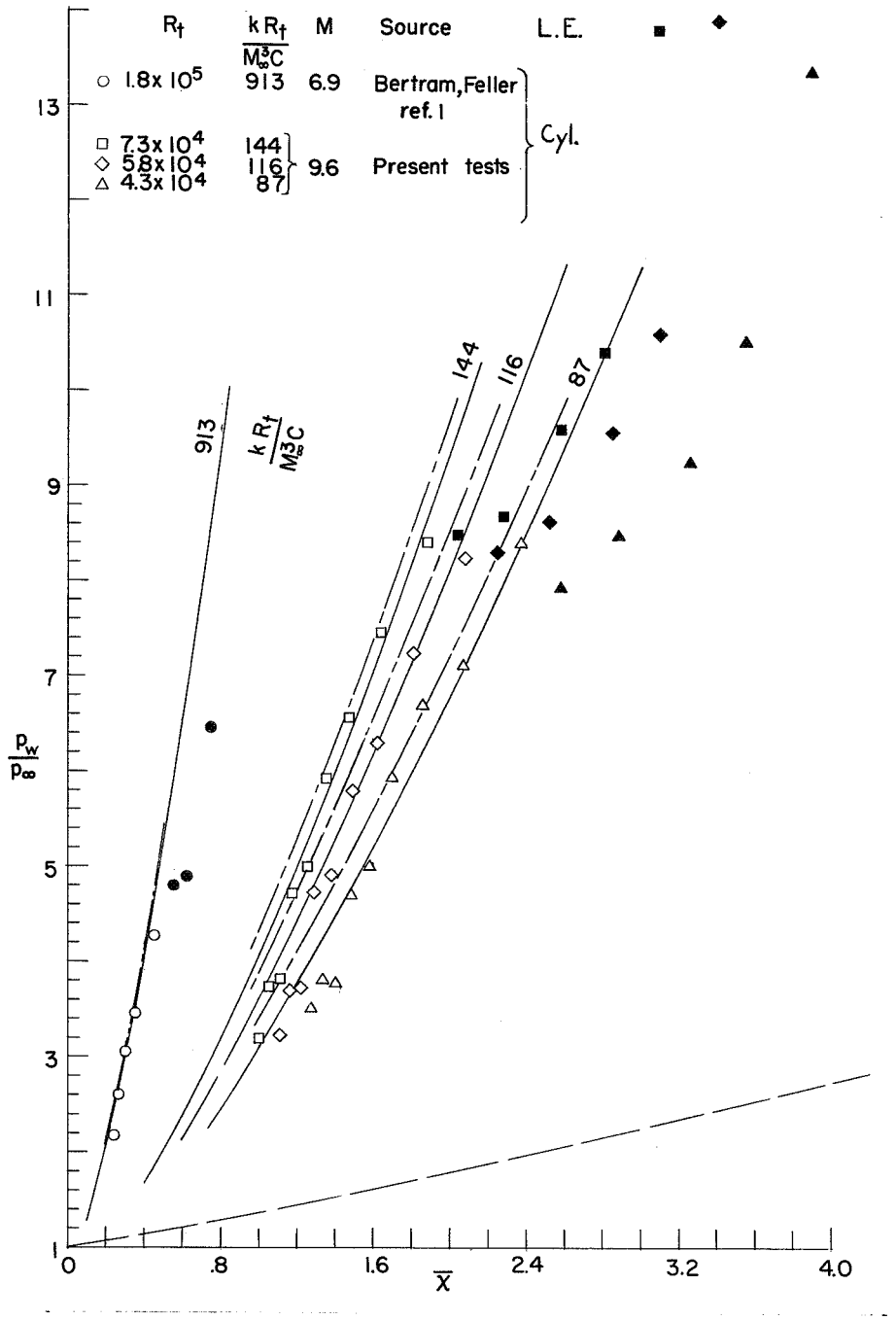

(d) $\frac{kR_t}{M_\infty^3 C}$ in range from about 87 to about 913.

Figure 8.- Concluded.

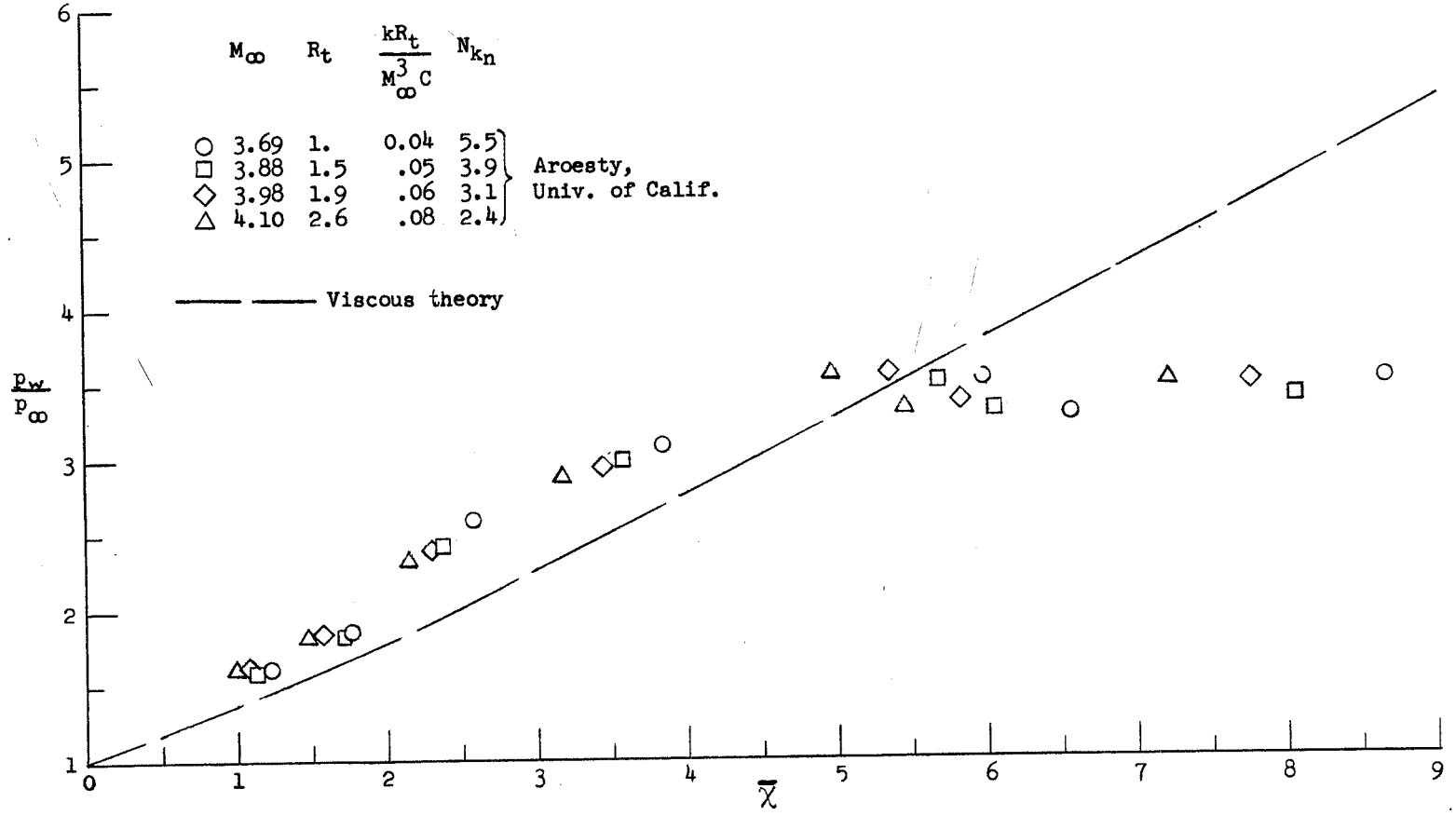

(a) $M_\infty \approx 3.9$.

Figure 9.- Effect of low-density flow on induced pressures in near-leading-edge region of flat plate.

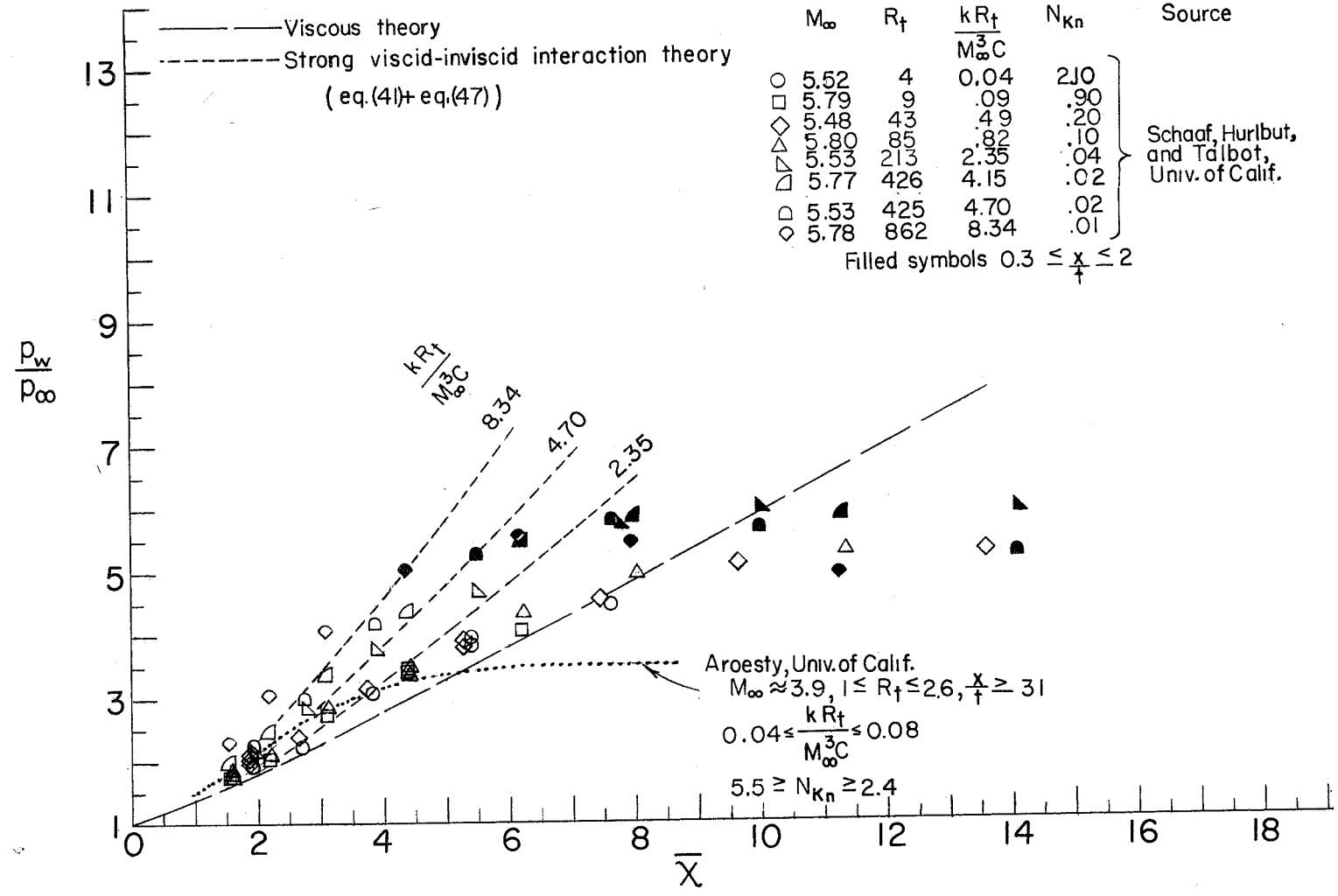

(b) $M_\infty \approx 5.7$.

Figure 9.- Concluded.

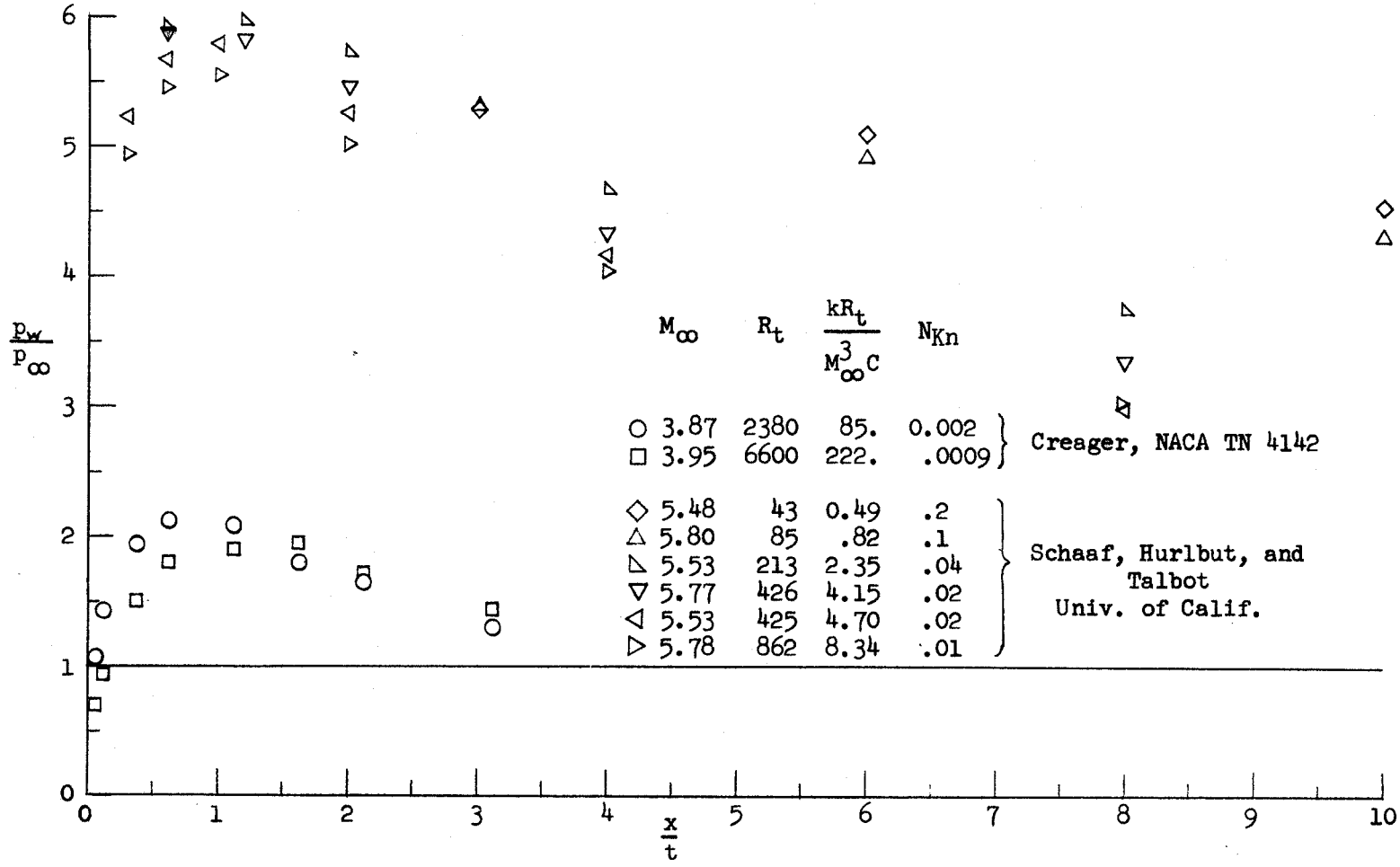

Figure 10.- Ratio of measured wall pressure to static pressure as a function of number of diameters downstream of flat leading edge of plate.

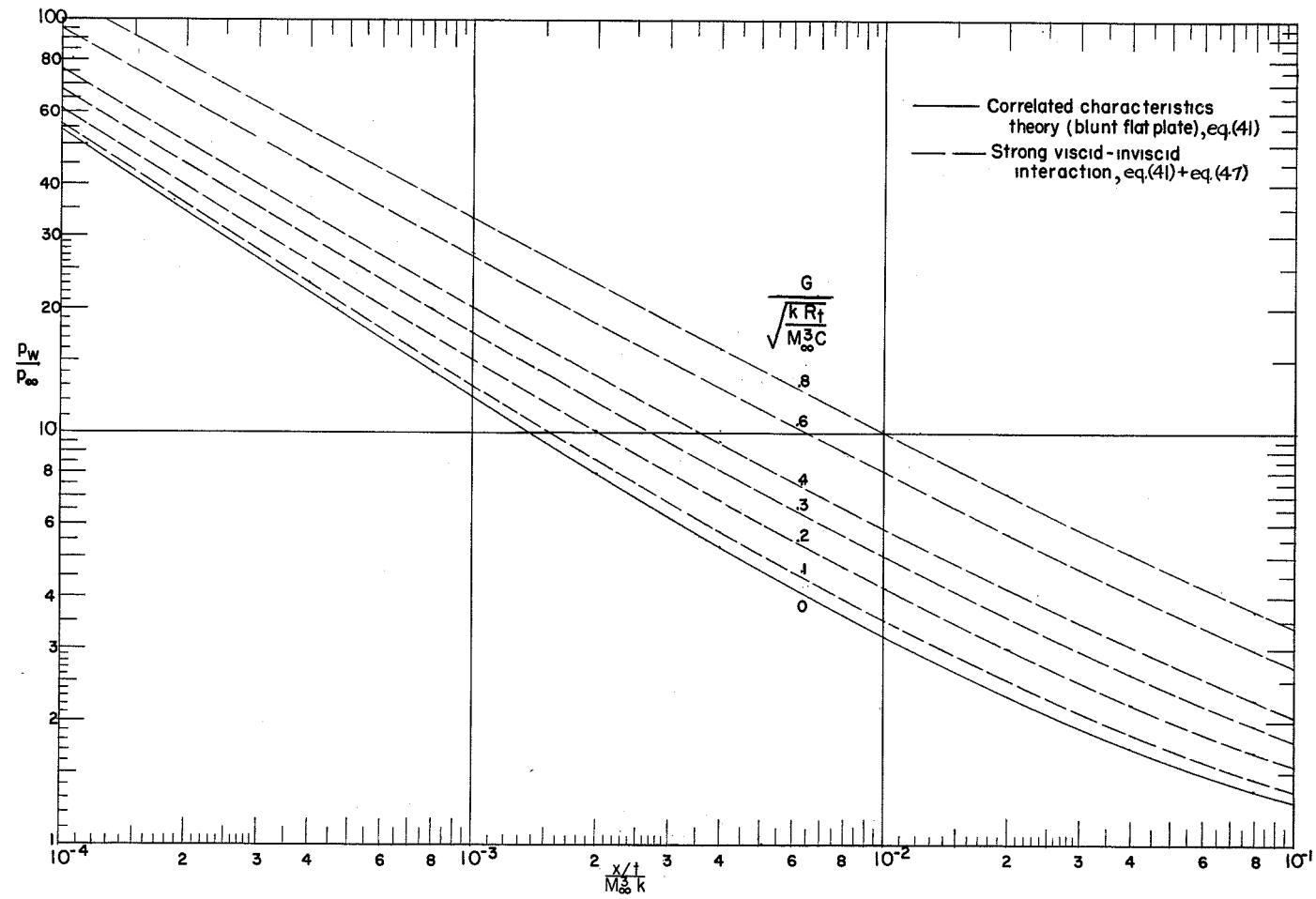

(a) $\gamma = 7/5$.

Figure 11.- Generalized chart showing effect on ratio of wall pressure to static pressure of interaction of boundary-layer displacement and blunt-leading-edge-induced effects on flat plate.

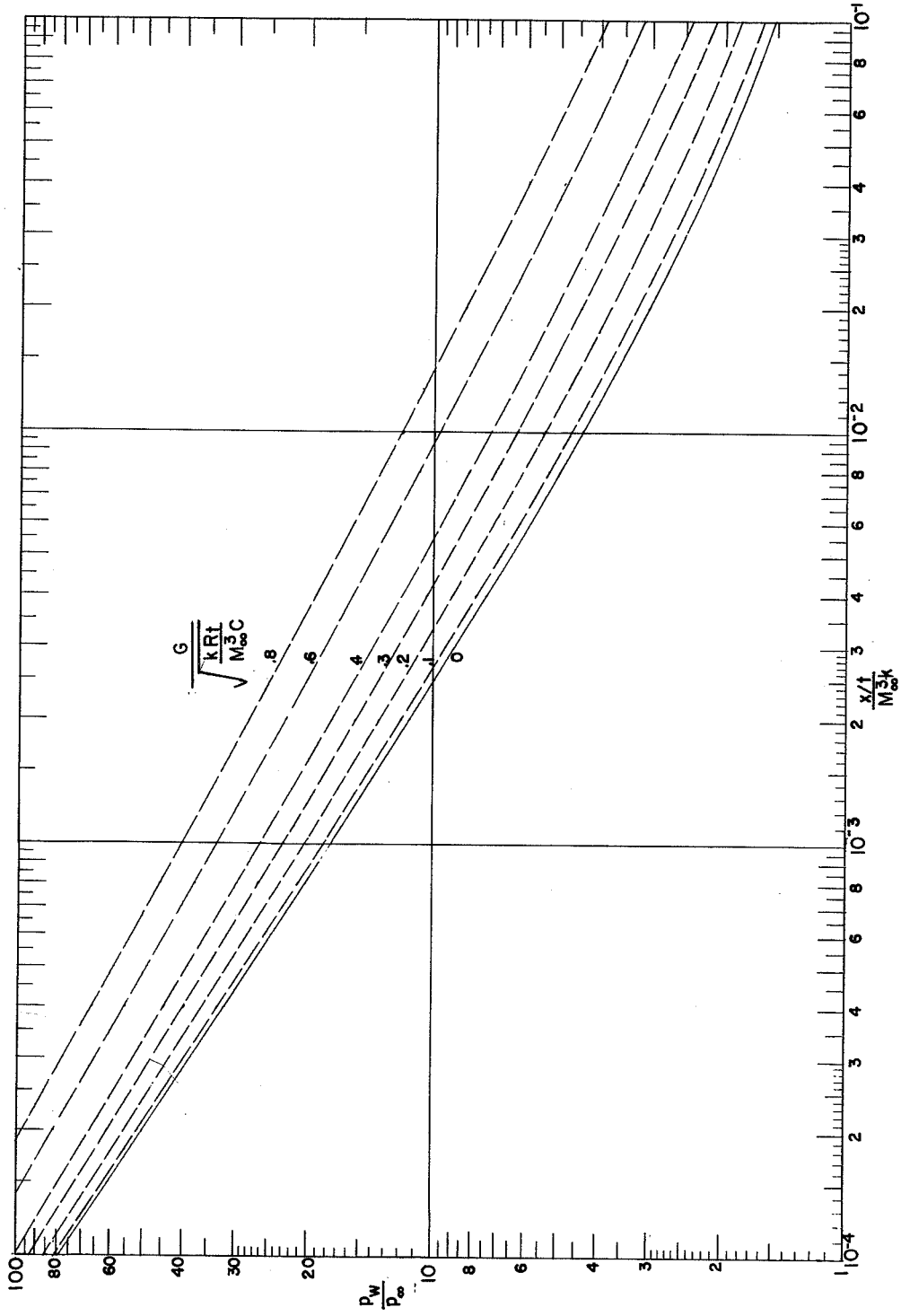

(b) $\gamma = 5/3$.

Figure 11.- Concluded.

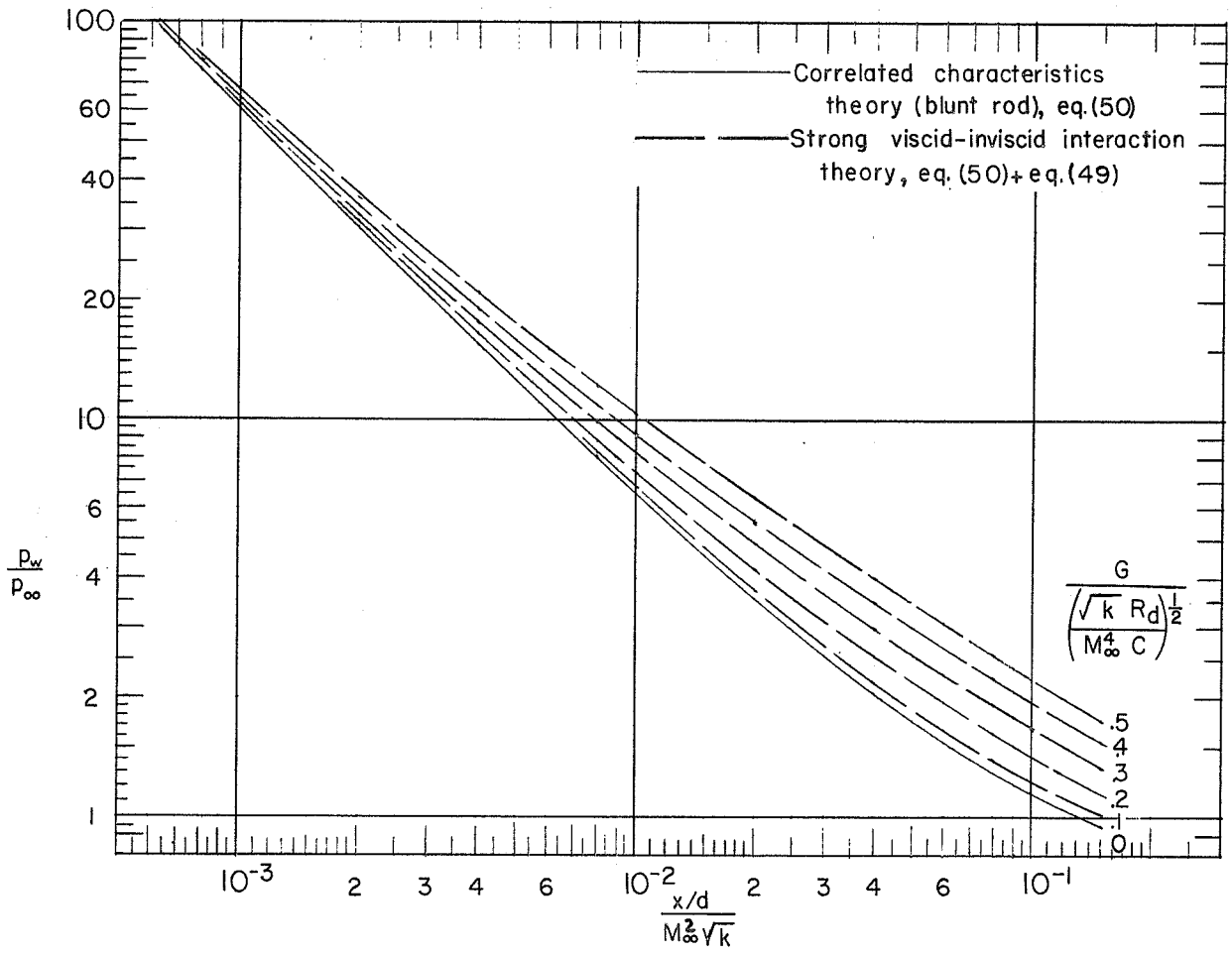

(a) $\gamma = 7/5$.

Figure 12.- Generalized chart showing effect on ratio of wall pressure to static pressure of interaction of boundary-layer displacement and blunt-nose-induced effects on rod.

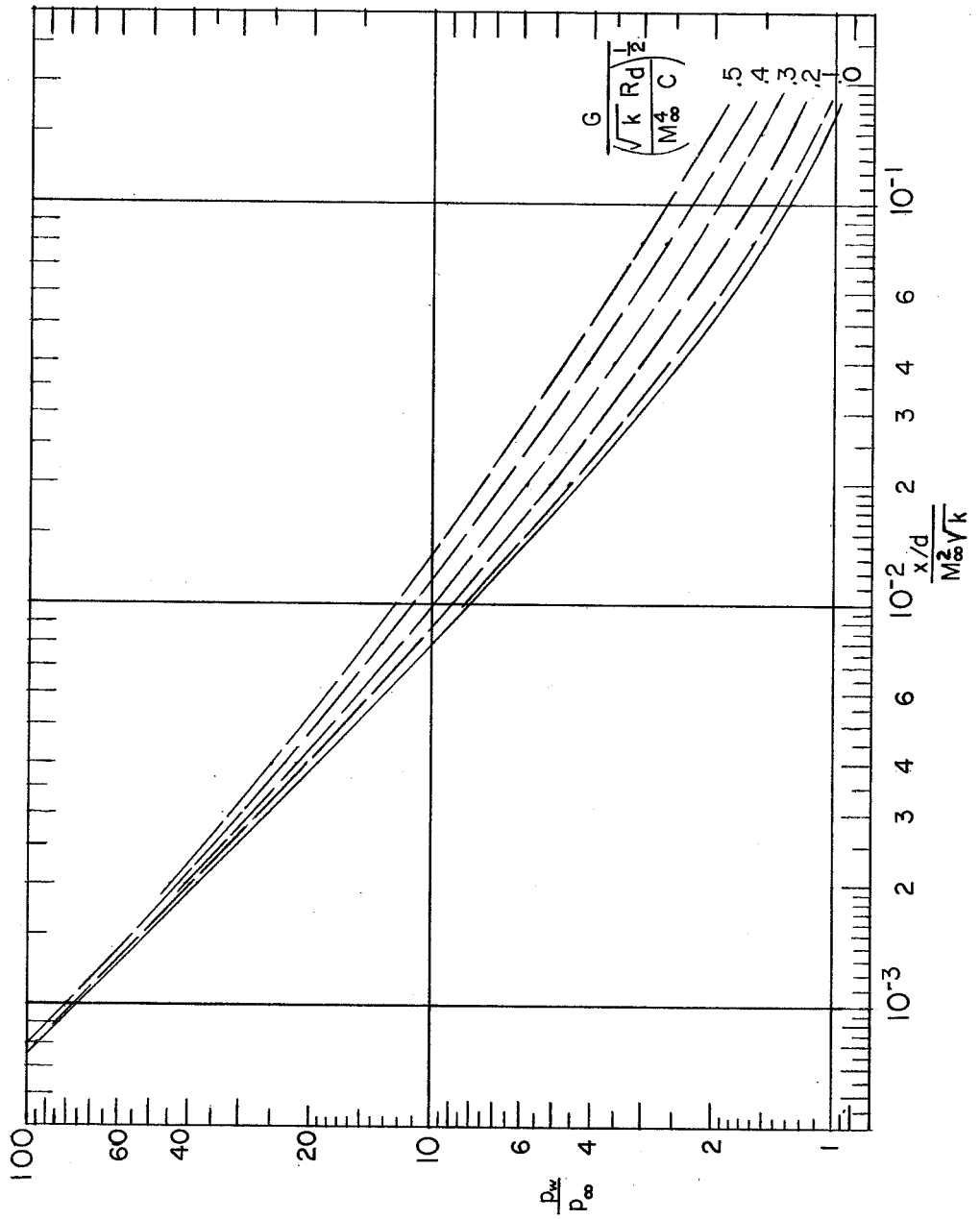

(b) $\gamma = 5/3$.

Figure 12.- Concluded.

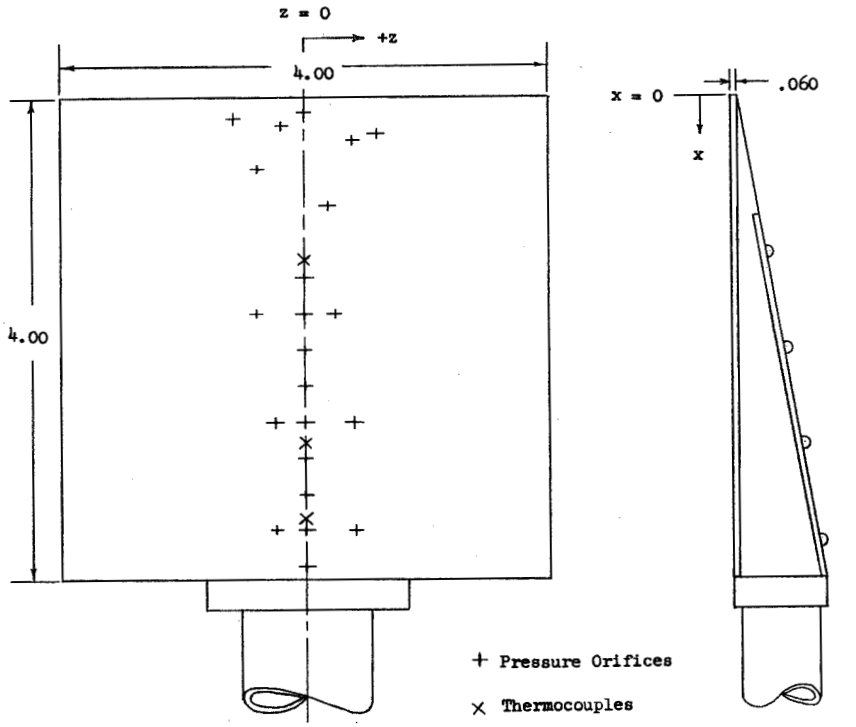

Pressure Orifice Locations

x	z
0.105	0
.172	−.588
.225	−.196
.300	+.588
.359	+.392
.595	−.392
.886	+.196
1.496	0
1.792	−.400
1.792	0
1.792	+.250
2.092	0
2.392	0
2.694	−.250
2.694	0
2.694	+.400
2.992	0
3.295	0
3.599	−.250
3.597	0
3.598	+.400
3.898	0

Thermocouple Locations

x	z
1.359	0
2.875	0
3.500	0

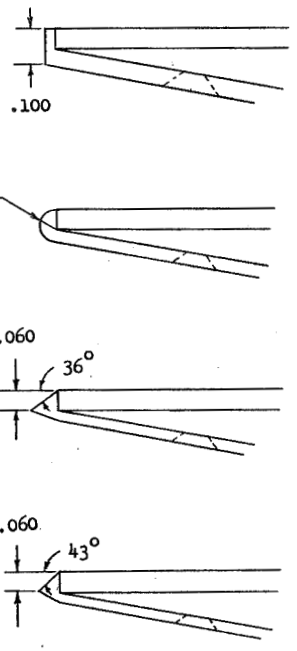

Figure 13.- Sketch of flat-plate model used in tests in Langley 11-inch hypersonic tunnel. All linear dimensions are in inches.

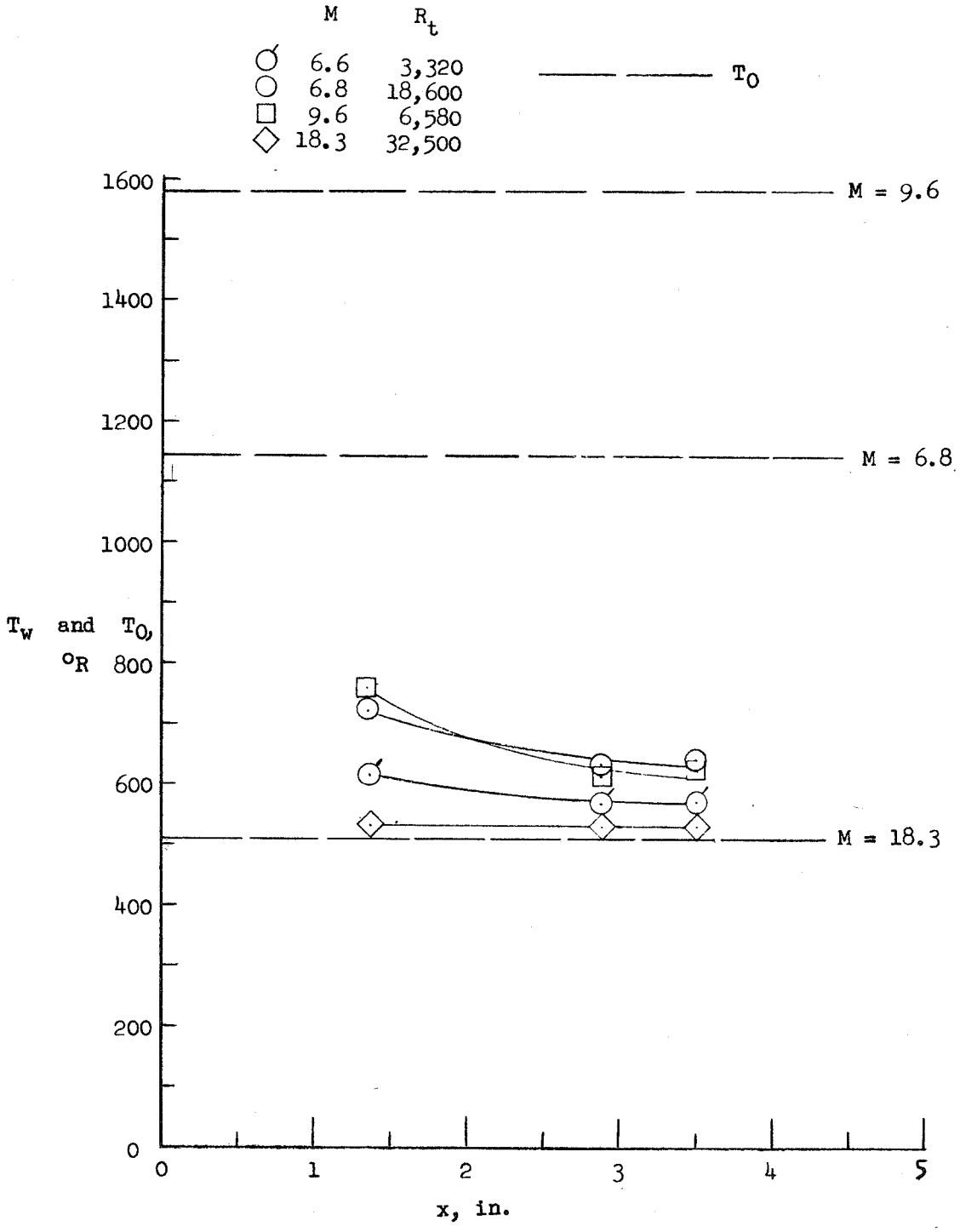

Figure 14.- Temperature distribution on flat plate with the 0.060-inch-thick flat-face leading edge.

L-1332